Journal of Mathematical Biology
https://doi.org/10.1007/s00285-020-01501-1

Mathematical Biology

Optimal open-loop desynchronization of neural oscillator populations

Dan Wilson[1]

Received: 26 September 2019 / Revised: 28 February 2020

Abstract
Deep brain stimulation (DBS) is an increasingly used medical treatment for various neurological disorders. While its mechanisms are not fully understood, experimental evidence suggests that through application of periodic electrical stimulation DBS may act to desynchronize pathologically synchronized populations of neurons resulting desirable changes to a larger brain circuit. However, the underlying mathematical mechanisms by which periodic stimulation can engender desynchronization in a coupled population of neurons is not well understood. In this work, a reduced phase-amplitude reduction framework is used to characterize the desynchronizing influence of periodic stimulation on a population of coupled oscillators. Subsequently, optimal control theory allows for the design of periodic, open-loop stimuli with the capacity to destabilize completely synchronized solutions while simultaneously stabilizing rotating block solutions. This framework exploits system nonlinearities in order to strategically modify unstable Floquet exponents. In the limit of weak neural coupling, it is shown that this method only requires information about the phase response curves of the individual neurons. The effects of noise and heterogeneity are also considered and numerical results are presented. This framework could ultimately be used to inform the design of more efficient deep brain stimulation waveforms for the treatment of neurological disease.

Keywords Floquet theory · Oscillators · Synchronization · Phase-amplitude reduction · Isostable coordinates · Optimal control · Neuroscience

Mathematics Subject Classification 92BXX · 37MXX · 41AXX · 34H05 · 34C15 · 92B25 · 49-XX

✉ Dan Wilson
dwilso81@utk.edu

[1] Department of Electrical Engineering and Computer Science, University of Tennessee, Knoxville, TN 37996, USA

Published online: 16 May 2020

1 Introduction

High-frequency deep brain stimulation (DBS) is a well-established treatment to alleviate the movement symptoms in patients with Parkinson's disease who do not respond well to medication (Benabid et al. 2009; Perlmutter and Mink 2006). However, despite its widespread use, the therapeutic mechanisms of high-frequency DBS are not well understood. This issue has hindered the development of more energy efficient and clinically effective stimulation protocols. While there is no consensus about the fundamental mechanisms of high-frequency DBS, it has long been known that relative to healthy individuals, local field potential recordings from patients with Parkinson's disease show a pronounced increase in the beta frequency range (from approximately 13–35 Hz) (Brown et al. 2001; Priori et al. 2004). Investigation of this phenomenon has led to the hypothesis that pathological synchronization among neurons in the basal ganglia-cortical loop contribute to both tremors and rigidity observed in patients with Parkinson's disease (Levy et al. 2002; Kühn et al. 2009; Kane et al. 2009; Hammond et al. 2007) and that high-frequency DBS actively mitigates the synchronization (Eusebio et al. 2011; Rosa et al. 2011; Kühn et al. 2008).

While it is still unknown whether excessive synchronization among neurons causes the movement symptoms of Parkinson's disease or is merely correlational, this hypothesis has led to the development of new stimulation strategies. For instance, real-time measurement of local field potential data has been used successfully in adaptive DBS stimulation protocols where the stimulation intensity is modulated based on measured beta power (Rosa et al. 2015; Little et al. 2013). Baseline local field potential recordings in patients with Parkinson's disease have also been used to identify suitable frequencies at which to apply high frequency DBS (Tsang et al. 2012). Additionally, Tass and colleagues have developed a stimulation protocol known as coordinated reset, whereby multiple stimulators are used to desynchronize a population of synchronized oscillators (Tass 2003; Manos et al. 2018); these stimulation protocols have shown promise as a treatment for Parkinson's disease in human (Adamchic et al. 2014) and nonhuman primate studies (Wang et al. 2016; Tass et al. 2012).

Experimental evidence that supports the notion that high-frequency DBS mitigates excessive synchronization associated with the symptoms of Parkinson's disease has spurred a search for efficient control strategies for achieving this objective. For instance, by constructing and analyzing stochastic phase maps and computing the associated Lyapunov exponents, Wilson et al. (2011) and Holt and Netoff (2014) suggest that chaotic desynchronization may occur when applying carefully tuned high frequency pulsatile stimulation when a nonzero variance is added to the spike times. Using a similar approach, Wilson and Moehlis (2015) found that for a wide range of periodic stimulation parameters, populations of neurons with a small amount of noise tend separate into identical and distinct clusters that are time-locked to the stimulation, a finding that is consistent with experimental observations that individual neural spikes appear time-locked to DBS pulses (Hashimoto et al. 2003; Bar-Gad et al. 2004; Cleary et al. 2013). Related studies have found that clustering of oscillator phases can emerge in populations of uncoupled oscillators subject to noise (Nakao et al. 2007). Feedback methods for disruption of neural synchronization have also been suggested. For instance, Matchen and Moehlis (2018) and Monga and Moehlis (2019) investi-

gate the possibility of using feedback control to actively separate a large population of synchronized neurons into clusters, Wilson and Moehlis (2014) develops a strategy to produce a positive finite time Lyapunov to engender chaotic desynchronization, and Nabi et al. (2013) suggests driving the neural population close to a phaseless set so that the neurons become desynchronized upon the subsequent relaxation to the limit cycle. For a detailed overview of phase reduction techniques used in many of the aforementioned applications, the interested reader is referred to Monga et al. (2019).

Because real-time feedback control on the time scales of individual neural spikes is not yet clinically possible, in this work attention will be restricted to periodic, open-loop stimulation. Here, a strategy is presented for finding a periodic DBS stimulus waveform that can stabilize unstable splay states in an oscillatory population of neurons. In the limit of small coupling and for an identical population of neurons, it is shown that periodic stimuli can be designed to stabilize rotating block solutions and splay states using only information about the phase response curves of individual neurons. The ability of this strategy to desynchronize a population of pathologically synchronized neurons is tested in both high and low noise environments, with qualitatively different results for each case. Additionally, the results to follow suggest fundamental limits on the number of rotating blocks that can be stabilized using periodic stimulation.

The organization of this paper is as follows: Sect. 2 gives background information on phase-amplitude reduction strategies that will be used for analysis of populations of coupled neurons. This background is presented in the context of the coupled oscillator models considered here. Section 3 presents new results that provide approximations for the phase-amplitude reduced dynamics for different periodic solutions of the weakly coupled oscillator models. Full derivations for the results from Sect. 3 are presented in Appendix A. Section 4 uses the results from Sect. 3 to develop conditions that can be used to modify the stability of periodic solutions in populations of coupled oscillators with periodic stimulation (without using state feedback). Appendix B summarizes an optimal control framework that is used to optimally satisfy the stability conditions from Sect. 4. Section 5 presents numerical results applied to populations of synaptically coupled neurons, considers the basins of attraction of stabilized periodic solutions, and investigates the stabilization results when non-negligible noise and oscillator heterogeneity are considered. Section 6 gives concluding remarks.

2 Background: isochrons and isostable coordinates of coupled oscillator models

This work will consider the behavior of synaptically coupled single-compartment neural models of the form

$$\begin{aligned}\dot{V}_i &= f_V(V_i, s_i, \boldsymbol{n}_i) + u(t) + \frac{g_{\text{syn}}}{N}\sum_{j=1}^{N} s_j(V_i - E_{\text{syn}}) \\ &= \underbrace{f_V(V_i, s_i, \boldsymbol{n}_i) + g_{\text{syn}} s_i(V_i - E_{\text{syn}})}_{\text{internal dynamics}} + \underbrace{u(t) + \frac{g_{\text{syn}}}{N}\sum_{j=1}^{N}(s_j - s_i)(V_i - E_{\text{syn}})}_{\text{external perturbations}},\end{aligned}$$

$$\begin{aligned}\dot{s}_i &= f_s(V_i, s_i),\\ \dot{\boldsymbol{n}}_i &= f_n(V_i, \boldsymbol{n}_i),\end{aligned} \tag{1}$$

where V_i is the transmembrane voltage of neuron i, s_i is a synaptic variable, and $\boldsymbol{n}_i \in \mathbb{R}^m$ are auxiliary variables (i.e., gating variables, ionic concentrations) which determine the neural dynamics, E_{syn} is the reversal potential of a given neurotransmitter, $g_{\text{syn}} < 0$ is the synaptic coupling strength, and $u(t)$ is an external current identically applied to all neurons so that the neurons fire periodically in steady state. In the transmembrane voltage equation, a distinction is made between the internal dynamics and external perturbations. In the absence of external perturbations, it is assumed that each neuron of the form (1) asymptotically approaches a T-periodic limit cycle $x^\gamma(t)$. Note that all neurons are assumed to be identical so that there is no dispersion in their natural frequencies. For a thorough discussion of neural models of the form (1), the interested reader is referred to Ermentrout and Terman (2010).

In order to aid in the analysis, phase reduction can be used to study (1) in a weakly perturbed setting (Ermentrout and Terman 2010; Izhikevich 2007; Winfree 2001):

$$\dot{\theta}_i = \omega + Z_V(\theta)\left[u(t) + \frac{g_{\text{syn}}}{N}\sum_{j=1}^{N}(s(\theta_j) - s(\theta_i))(V(\theta_i) - E_{\text{syn}})\right]. \tag{2}$$

Here $\theta_i \in [0, 2\pi)$ denotes the phase of oscillator i giving a sense of the state of the ith oscillator in reference to its periodic orbit. Here, $\theta_i = 0$ is chosen to correspond to the moment neuron i fires. Additionally, $Z_V(\theta)$ is the phase response curve PRC of a single neuron in response to voltage perturbations, and $\omega = 2\pi/T$ is the natural frequency of each neuron. The PRC is calculated with respect to $x^\gamma(t)$. The reduction (2) is most accurate when the Floquet multipliers associated with the periodic orbits of the neurons are close to zero so that perturbations rapidly decay to the limit cycle.

Because $\theta_i \in \mathbb{S}^1$, intuitively one can think of the phase of each neuron traveling around a ring. If the neurons are synchronized, the neurons fire at the same time. It will be assumed throughout this work that the coupling is such that in the absence of stimulation, the synchronized state is asymptotically stable. Using the reduced model (2) as a starting point, strategies will be developed to destabilize a synchronized state comprised of N identical neurons in favor of the splay state (with phases of all neurons spread equally around the ring) or rotating block states (having N/G blocks of G oscillators with the phases of the blocks spread equally around the ring). Figure 1 gives a pictorial example of these states. The reduced model (2) will be used as a starting point to achieve this control objective.

2.1 Background: phase amplitude reduction of weakly coupled oscillators

Consider a more general form of (2)

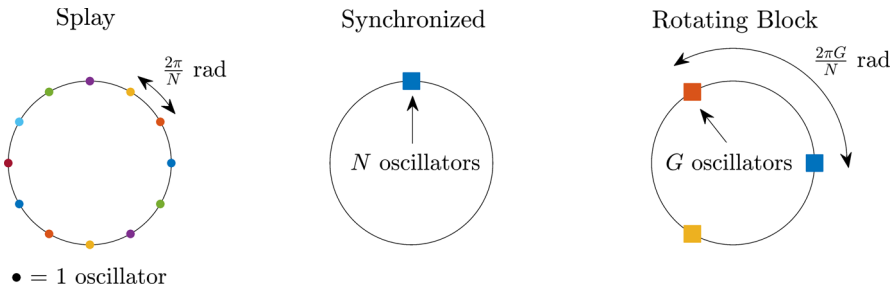

Fig. 1 For splay solutions, the phases of N oscillators are spaced equally around the ring. For synchronized solutions, all N oscillators have identical phases. For the rotating block solution, each block contains G oscillators and the blocks are spaced equally around the ring

$$\dot{\theta}_i = \omega + \frac{1}{N} Z_V(\theta_i) \sum_{j=1}^{N} f(\theta_i, \theta_j) + Z_V(\theta_i) u(t), \tag{3}$$

where $f(a, b)$ characterizes the coupling and the network is connected in an all-to-all manner. Note here that all oscillators and coupling functions are assumed to be identical so that Z_V, ω, and f are the same for all neurons. Additionally, $u(t)$ is applied identically to each oscillator. Much work has been done on understanding the collective behavior of a population (3) due to input (Ko and Ermentrout 2009; Kawamura et al. 2008; Levnajić and Pikovsky 2010; Kotani et al. 2014). Provided (3) has a periodic solution $X^\gamma(t) = \left[\theta_1^\gamma(t) \ldots \theta_N^\gamma(t)\right]^T$, one commonly used approach is to apply a secondary phase reduction to (3), transforming it into an equation of the form

$$\dot{\Theta} = \Omega + \boldsymbol{Z}^T(\Theta) \boldsymbol{P}(t), \tag{4}$$

where Θ is the population phase, $\boldsymbol{Z}(\Theta) \in \mathbb{R}^N$ is the population PRC, Ω is the natural frequency of the collective oscillation, and $\boldsymbol{P}(t) = u(t)\left[Z_V(\theta_1) \ldots Z_V(\theta_N)\right]^T$ is the effective perturbation. Equation (4) is simply a phase reduction performed on the model (3) when considering each $Z_V(\theta_i)u(t)$ as a weak external input. Such a reduction was considered for general coupling functions (Nakao et al. 2018). The population phase Θ, gives a sense of the state of the collective oscillation with respect to the periodic solution $X^\gamma(t)$. Note here that the periodic orbit $X^\gamma(t)$ does not need to be a synchronized solution. Because $f(\theta_i, \theta_j)$ is assumed to be an order ϵ term, one can show that $\Omega = \omega + \mathcal{O}(\epsilon)$. While this reduction approach reduces the dimension of (2) from N to one making analysis more tractable, a significant drawback is that it ignores the slow decay of perturbations back to the limit cycle thereby limiting its practical utility when perturbations become larger. Here, a related approach will be used where (3) is represented with a phase-amplitude reduction (Wilson and Ermentrout 2018,

2019),

$$\begin{aligned}\dot{\Theta} &= \Omega + \boldsymbol{Z}^T(\Theta)\boldsymbol{P}(t) + \sum_{k=1}^{\beta}\left[\boldsymbol{B}^{k\,T}(\Theta)\psi_k\right]\boldsymbol{P}(t),\\ \dot{\psi}_j &= \kappa_j\psi_j + \boldsymbol{I}_j^T(\Theta)\boldsymbol{P}(t) + \sum_{k=1}^{\beta}\left[\boldsymbol{C}_j^{k\,T}(\Theta)\psi_k\right]\boldsymbol{P}(t),\\ &\quad j = 1,\ldots,\beta. \end{aligned} \tag{5}$$

Above, ψ_j are isostable coordinates which give a sense of the distance from the limit cycle solution, κ_j is the corresponding non-zero Floquet exponent (Jordan and Smith 2007) ordered so that $\text{Real}(\kappa_1) > \text{Real}(\kappa_2) > \cdots > \text{Real}(\kappa_\beta)$, $\boldsymbol{I}_j(\Theta)$ is the population isostable response curve (analogous to the population PRC), $\boldsymbol{B}^k(\Theta)$, and $\boldsymbol{C}_j^k(\Theta)$ provide second order corrections to the phase and isostable dynamics, respectively, and $\beta \leq N-1$ is the number of isostable coordinates considered in the reduction. Typically, isostable coordinates ψ_j with associated $\text{Real}(\kappa_j) \ll 0$ (i.e., those that rapidly decay) are taken to be close enough to zero so that they can be neglected in the reduction (5) (Wilson and Ermentrout 2018).

As investigated in Wilson and Ermentrout (2019), it is also possible to apply the phase-amplitude reduction strategy directly to (1) without using the intermediate reduction (3). The resulting reduction takes the form

$$\begin{aligned}\dot{\Theta} &= \Omega + \mathcal{Z}(\Theta)u(t) + \sum_{k=1}^{\beta}\left[\mathcal{B}^k(\Theta)\psi_k\right]u(t),\\ \dot{\psi}_j &= \kappa_j\psi_j + \mathcal{I}_j(\Theta)u(t) + \sum_{k=1}^{\beta}\left[\mathcal{C}_j^k(\Theta)\psi_k\right]u(t),\\ &\quad j = 1,\ldots,\beta. \end{aligned} \tag{6}$$

where $\mathcal{Z}(\Theta) \equiv \sum_{i=1}^{N}\frac{\partial\Theta}{\partial V_i}$, $\mathcal{I}_j(\Theta) = \sum_{i=1}^{N}\frac{\partial\psi_j}{\partial V_i}$, $\mathcal{B}^k(\Theta) \equiv \sum_{i=1}^{N}\frac{\partial^2\Theta}{\partial\psi_k\partial V_i}$ and $\mathcal{C}_j^k(\Theta) \equiv \sum_{i=1}^{N}\frac{\partial^2\psi_j}{\partial\psi_k\partial V_i}$ and all partial derivatives are evaluated at phase Θ on the periodic orbit. Provided (2) is a good approximation of (1), as illustrated in Wilson and Ermentrout (2019), $\mathcal{Z}(\Theta)u(t) \approx \boldsymbol{Z}^T(\Theta)\boldsymbol{P}(t)$, $\mathcal{I}_j(\Theta)u(t) \approx \boldsymbol{I}_j^T(\Theta)\boldsymbol{P}(t)$, $\mathcal{B}^k(\Theta)u(t) \approx \boldsymbol{B}^{k\,T}(\Theta)\boldsymbol{P}(t)$ and $\mathcal{C}_j^k(\Theta)u(t) \approx \boldsymbol{C}_j^{k\,T}(\Theta)\boldsymbol{P}(t)$. In the sections to follow it will be shown using (5) that in the limit of small coupling, the terms of the reduction (5) [and hence the terms of the reduction (6)] can be found with only knowledge of $Z_V(\theta)$ in many cases.

2.2 Background: isochrons, isostables, and Floquet theory

For stable limit cycles, the phase Θ in Eq. (5) gives a sense of the asymptotic behavior of (2) during its approach to the limit cycle using the notion of isochrons (Guckenheimer 1975; Winfree 2001). Isochrons can be used to extend the notion of phase to the basin of attraction of the limit cycle and are defined as follows: for an initial condition $\boldsymbol{X}(0)$ on a limit cycle of (3) the corresponding isochron is the set of all $\boldsymbol{Y}(0)$ such that

$$\lim_{t\to\infty} ||\boldsymbol{X}(t) - \boldsymbol{Y}(t)|| = 0, \tag{7}$$

where $||\cdot||$ can be any norm. In this work, unstable limit cycles will also be of interest, requiring the nonstandard definition of phase used in Wilson (2019b). This definition is only valid near the T-periodic limit cycle solution $\boldsymbol{x}^\gamma(t)$ where the dynamics can be approximated as

$$\frac{d\Delta\boldsymbol{x}(t)}{dt} = J(\boldsymbol{x}^\gamma(t))\Delta\boldsymbol{x} + \mathcal{O}\big(|\Delta\boldsymbol{x}|^2\big). \tag{8}$$

Here $\Delta\boldsymbol{x}(t) = \boldsymbol{x}(t) - \boldsymbol{x}^\gamma(t)$ with $\boldsymbol{x}(t) \equiv [\theta_1(t)\ \ldots\ \theta_N(t)]^T$ and $J(\boldsymbol{x}^\gamma(t))$ represents the Jacobian of (2) evaluated at $\boldsymbol{x}^\gamma(t)$. Because $\boldsymbol{x}^\gamma(t)$ is periodic to leading order in $\Delta\boldsymbol{x}$, the solutions of (8) can be characterized using Floquet theory (Grimshaw 1993; Jordan and Smith 2007) according to

$$\boldsymbol{x}(t) = \boldsymbol{x}^\gamma(t) + \sum_{j=1}^{N-1} c_j \exp(\kappa_j t)\boldsymbol{q}_j(t), \tag{9}$$

Here c_j are constants chosen to satisfy initial conditions, κ_j are the non-zero Floquet exponents, and $\boldsymbol{q}_j(t)$ are T-periodic functions. Note that the term $c_N\boldsymbol{q}_N(t)$ (corresponding by definition to Floquet exponent $\kappa_N = 0$) is absorbed into $\boldsymbol{x}^\gamma(t)$. As in Wilson (2019b), (9) can be used to provide an alternate definition of phase, where the $\Theta = 0$ level set, Γ_0 is defined as

$$\Gamma_0 = \left\{ \boldsymbol{x} \in \mathbb{R}^n | \boldsymbol{x} = \boldsymbol{x}^\gamma(0) + \sum_{j=1}^{N-1} c_j \boldsymbol{q}_j(0) \right\}. \tag{10}$$

Consequently, phase at all locations near the periodic orbit will be defined by

$$\Theta(x) = \frac{2\pi(T - t_\Gamma)}{T}, \tag{11}$$

where t_Γ is the time at which Γ_0 is first crossed under the fully nonlinear flow. Likewise, isostable coordinates can be defined for unstable periodic orbits according to

$$\psi_j(\boldsymbol{x}) = \boldsymbol{w}_j^T(\boldsymbol{x}_\Gamma - \boldsymbol{x}_0)\exp(-\kappa_j t_\Gamma), \tag{12}$$

where $\boldsymbol{x}_\Gamma$ is the location at which Γ_0 is first crossed under the fully nonlinear flow and $\boldsymbol{w}_j$ is defined such that $\boldsymbol{w}_j^T \boldsymbol{q}_i(0) = 1$ for $i = j$ and 0 otherwise. As shown in Wilson (2019b) when using the definition (11) there is an order $|\Delta \boldsymbol{x}|^2$ discontinuity in the phase and isostable coordinates across the Γ_0 level set which can be ignored provided $\boldsymbol{x}(t)$ is close enough to the periodic orbit.

Using the definition (12) and the approximate solution (9), one can show that to leading order in $|\Delta \boldsymbol{x}|$, the constant c_j is equivalent to $\psi_j(\boldsymbol{x})$. This allows (9) to be written in terms of the phase and isostable coordinates (cf. Wilson 2019b; Wilson and Ermentrout 2018)

$$\boldsymbol{x}(t) = \boldsymbol{x}^\gamma(\theta(t)) + \sum_{j=1}^{N-1} \psi_j \boldsymbol{q}_j(\theta(t)). \tag{13}$$

In this work, the definitions (11) and (12) will be used in the phase-amplitude reductions. Functions $\boldsymbol{Z}(\Theta)$, $\boldsymbol{I}_j(\Theta)$, $\boldsymbol{B}^k(\Theta)$, and $\boldsymbol{C}_j^k(\Theta)$ (in addition to $\mathcal{Z}(\Theta), \mathcal{I}_j(\Theta), \mathcal{B}^k(\Theta)$ and $\mathcal{C}_j^k(\Theta)$) can be computed numerically using methods detailed in Wilson (2019a).

2.3 Background: stabilization and destabilization using periodic stimulation

The stability of periodic solutions of (3) is determined by the Floquet exponents. One Floquet exponent will always be equal to zero due to periodicity of solutions. If the remaining κ_j have real components that are strictly less than zero the periodic orbit is stable, otherwise, it is unstable. Wilson (2019b) provides a strategy to modify the Floquet exponents using periodic stimulation with results summarized here.

Starting with the phase-amplitude reduction (5) suppose that $\boldsymbol{P}(t)$ is a T_p-periodic perturbation. Additionally, changing to a rotating reference frame with the relation $\eta = \Theta - \Omega_p t$ where $\Omega_p = 2\pi/T_p$ yields

$$\begin{aligned}
\dot{\eta} &= \Delta\Omega + \boldsymbol{Z}^T(\eta + \Omega_p t)\boldsymbol{P}(t) + \sum_{k=1}^{\beta} \left[\boldsymbol{B}^{k\,T}(\eta + \Omega_p t)\psi_k\right]\boldsymbol{P}(t), \\
\dot{\psi}_j &= \kappa_j \psi_j + \boldsymbol{I}_j^T(\eta + \Omega_p t)\boldsymbol{P}(t) + \sum_{k=1}^{\beta} \left[\boldsymbol{C}_j^{k\,T}(\eta + \Omega_p t)\psi_k\right]\boldsymbol{P}(t), \\
& j = 1, \ldots, \beta.
\end{aligned} \tag{14}$$

where $\Delta\Omega \equiv \Omega - \Omega_p$ and is assumed to be an $\mathcal{O}(\epsilon)$ term. Equation (14) is T_p-periodic and of the general form $\dot{\boldsymbol{y}} = \epsilon Q(\boldsymbol{y}, t)$ so that the method of averaging can be used (Sanders et al. 2007; Guckenheimer and Holmes 1983) allowing for the approximation of (14) as

$$\dot{H} = \Delta\Omega + \rho(H) + \sum_{k=1}^{\beta} \Psi_k \zeta_k(H)$$

$$\dot{\boldsymbol{y}} = (D + E(H))\boldsymbol{y} + \boldsymbol{q}(H), \tag{15}$$

where

$$\boldsymbol{y} = \begin{bmatrix} \Psi_1 \\ \Psi_2 \\ \vdots \\ \Psi_\beta \end{bmatrix}, \quad D = \begin{bmatrix} \kappa_1 & & & \\ & \kappa_2 & & \\ & & \ddots & \\ & & & \kappa_\beta \end{bmatrix}, \quad E(H) = \begin{bmatrix} \nu_{1,1}(H) & \nu_{1,2}(H) & \dots & \nu_{1,\beta}(H) \\ \nu_{2,1}(H) & \nu_{2,2}(H) & \dots & \nu_{2,\beta}(H) \\ \vdots & \vdots & \ddots & \vdots \\ \nu_{\beta,1}(H) & \nu_{\beta,1}(H) & \dots & \nu_{\beta,\beta}(H) \end{bmatrix},$$

$$\boldsymbol{q}(H) = \begin{bmatrix} \mu_1(H) \\ \mu_2(H) \\ \vdots \\ \mu_\beta(H) \end{bmatrix},$$

and $\rho(H) = \frac{1}{T_p}\int_0^{T_p} \boldsymbol{Z}^T(H + \Omega_p t)\boldsymbol{P}(t)dt$, $\zeta_k(H) = \frac{1}{T_p}\int_0^{T_p} \boldsymbol{B}^k(H + \Omega_p t)\boldsymbol{P}(t)dt$, $\nu_{j,k}(H) = \frac{1}{T_p}\int_0^{T_p} \boldsymbol{C}_j^k(H + \Omega_p t)\boldsymbol{P}(t)dt$, and $\mu_k(H) = \frac{1}{T_p}\int_0^{T_p} \boldsymbol{I}_k(H + \Omega_p t)\boldsymbol{P}(t)dt$. Fixed points of (15) correspond to periodic orbits of (14) with the same stability (Sanders et al. 2007; Guckenheimer and Holmes 1983).

As investigated in Wilson (2019b), (15) has a stable fixed point provided some H_0 exists for which

$$\rho(H_0) = -\Delta\Omega, \tag{16}$$

$$d\rho/dH|_{H_0} < 0, \tag{17}$$

$$\mu_i(H_0) = 0 \quad \text{for } i = 1, \dots, \beta, \tag{18}$$

$$\Lambda(D + E(H_0)) < 0, \tag{19}$$

where $\Lambda(R)$ is the maximum real component of any eigenvalue of the matrix R. Consequently, these conditions were used in Wilson (2019b) as design parameters to stabilize unstable periodic orbits. Condition (19) can be rewritten assuming that the matrix $E(H)$ is a small perturbation and that the eigenvalues of matrix D are not repeated. With these assumptions, as shown in Wilson (2019b), condition (19) can be rewritten as

$$\text{real}(\kappa_i + \nu_{i,i}) < 0 \quad \text{for } i = 1, \dots, \beta. \tag{20}$$

As will be shown here, more detailed analysis of the averaged equations (15) can be used to design periodic inputs that can either stabilize or destabilize periodic solutions of (2) as desired. In Appendix B it is shown how any combination of conditions (16)–(18) and (20) can be satisfied in an energy-optimal manner. Finally, note that identical conditions for stabilization of periodic orbits of (6) can be determined by repeating the above arguments using $\mathcal{Z}(\Theta)u(t)$, $\mathcal{I}_j(\Theta)u(t)$, $\mathcal{B}^k(\Theta)u(t)$ and $\mathcal{C}_j^k(\Theta)u(t)$ in place of $\boldsymbol{Z}^T\boldsymbol{P}(t)$, $\boldsymbol{I}_j^T(\Theta)\boldsymbol{P}(t)$, $\boldsymbol{B}^{k^T}(\Theta)\boldsymbol{P}(t)$ and $\boldsymbol{C}_j^{k^T}(\Theta)\boldsymbol{P}(t)$, respectively.

For large populations of coupled oscillators, the dimensionality of the phase-amplitude reduced equations (5) can still be quite high. Directly attempting to use

this strategy to satisfy (16)–(19) would be a difficult task. However, as shown in the analysis below, a greatly simplified set of conditions can be derived for some general categories of periodic solutions of (3). Furthermore, as will be shown in the following sections, stabilization (and destabilization) of periodic solutions can be achieved solely with knowledge of the PRC of the individual oscillators (i.e., $Z_V(\theta)$).

3 Approximation of phase-amplitude reduced equations for weakly coupled oscillators

In this work, the primary concern is understanding how periodic, nonfeedback stimulation can modify the stability of periodic solutions of (2). From conditions (16)–(19), this can be done with knowledge of $\boldsymbol{Z}(\Theta)$, $\boldsymbol{I}_k(\theta)$, and $\boldsymbol{C}_j^k(\theta)$ from the reduction (14). In general, these reduced functions can be derived using methods given in Wilson (2019a). However, as newly shown in this work, in the limit of weak coupling many of these terms can be related directly to $Z_V(\theta)$, the PRCs of the individual oscillators.

To do so, consider a periodic solution $\theta_k^{\text{per}}(t)$ of (3) that emerges when $u(t) = 0$ for which $\theta_k^{\text{per}}(t) = \theta_k^{\text{per}}(t+T)$ for some $T = 2\pi/\Omega$ for all k. By assuming that coupling $f(\theta_i, \theta_j)$ is an order ϵ term where $0 < \epsilon \ll 1$ asymptotic expansion in powers of ϵ can be used to show that $\theta_i^{\text{per}}(t) = \theta_i^{\text{per}}(0) + \omega t + \mathcal{O}(\epsilon)$. Thus, $\theta_j^{\text{per}} = \theta_i^{\text{per}} + \eta_{i,j} + \mathcal{O}(\epsilon)$ where $\eta_{j,i}$ is a constant. Under these assumptions, as shown in Appendix A, the population response curves take the form:

$$\boldsymbol{Z}^T(\Theta)\boldsymbol{P}(t) = \frac{u(t)}{\boldsymbol{w}_N^T\mathbf{1}}\sum_{j=1}^{N}\left[Z_V(\theta_j^{\text{per}}(\Theta))w_N^j\right], \tag{21}$$

$$\boldsymbol{I}_j^T(\Theta)\boldsymbol{P}(t) = \sum_{i=1}^{N}\left[w_j^i Z_V(\theta_i^{\text{per}}(\Theta))\right]u(t), \tag{22}$$

$$\boldsymbol{C}_j^{k\,T}(\Theta)\boldsymbol{P}(t) = \sum_{i=1}^{N}\left[w_j^i v_k^i Z_V'(\theta_i^{\text{per}}(\Theta))\right]u(t), \tag{23}$$

where $\boldsymbol{w}_j$, $\boldsymbol{v}_j$, and λ_j are left eigenvectors, right eigenvectors, and eigenvalues, respectively of

$$M = \frac{1}{N}\begin{bmatrix} A_1 + B(0) & B(\eta_{1,2}) & \dots & B(\eta_{1,N}) \\ B(\eta_{2,1}) & A_2 + B(0) & \dots & B(\eta_{2,N}) \\ \vdots & & \ddots & \vdots \\ B(\eta_{N,1}) & B(\eta_{N,2}) & \dots & A_N + B(0) \end{bmatrix} \tag{24}$$

where,

$$A_i \equiv \frac{1}{T}\int_0^T\left[Z_V'(\omega t)\sum_{j=1}^{N} f(\omega t, \omega t + \eta_{i,j}) + Z_V(\omega t)\sum_{j=1}^{N} f_a(\omega t, \omega t + \eta_{i,j})\right]dt,$$

$$B(\eta_{i,j}) \equiv \frac{1}{T}\int_0^T \left[Z_V(\omega t) f_b(\omega t, \omega t + \eta_{i,j}) \right] dt.$$

A full derivation of (21)–(23) is presented in Appendix A where it is also shown that the eigenvalues of the matrix M correspond directly to the Floquet exponents from (9). In the subsections to follow, relationships (21)–(23) are examined specifically for splay, synchronous, and rotating block solutions. The resulting simplifications will serve as a foundation to investigate stability conditions for periodic input in the sections to follow.

3.1 Reduced equations for specific periodic solutions

Splay state solutions One solution of general interest is the splay state, for which the phases of all oscillators are spaced equally as shown in Fig. 1. For such a solution, as shown Appendix A.1 some useful simplifications are possible

$$\boldsymbol{Z}^T(\Theta)\boldsymbol{P}(t) = \frac{u(t)}{N}\sum_{j=1}^{N}\left[Z_V\left(\Theta + \frac{2(j-1)\pi}{N}\right)\right], \tag{25}$$

$$\boldsymbol{C}_j^{jT}(\Theta)\boldsymbol{P}(t) = \frac{u(t)}{N}\sum_{i=1}^{N}\left[Z_V'\left(\Theta + \frac{2(j-1)\pi}{N}\right)\right]. \tag{26}$$

The isostable response curves do not admit any significant simplifications beyond (22) for splay state solutions.

Synchronous solutions For a periodic synchronous solution, the phases of all oscillators are equal. For such a solution, as shown in Appendix A.2

$$\boldsymbol{Z}^T(\Theta)\boldsymbol{P}(t) = u(t)Z_V(\Theta), \tag{27}$$

$$\boldsymbol{I}_j^T(\Theta)\boldsymbol{P}(t) = 0, \tag{28}$$

$$\boldsymbol{C}_j^{kT}(\Theta)\boldsymbol{P}(t) = \begin{cases} u(t)Z_V'(\Theta), & \text{if } j = k, \\ 0, & \text{otherwise.} \end{cases} \tag{29}$$

Rotating block solutions For a large population of oscillators, the full splay state may be difficult to stabilize. In this case, rotating block solutions are of interest, whereby N/G blocks of G oscillators are spaced equally in phase (see, for example, Fig. 1). As shown in Appendix A.3 reduced equations of the rotating block solutions with 2 blocks are markedly similar to those of the splay solution when only 2 oscillators are considered with the following reduced equations

$$\boldsymbol{Z}^T(\Theta)\boldsymbol{P}(t) = \frac{u(t)}{2}\left[Z_V(\Theta) + Z_V(\Theta+\pi)\right], \tag{30}$$

$$\boldsymbol{I}_k^T(\Theta)\boldsymbol{P}(t) = \begin{cases} \frac{u(t)\sqrt{N}}{2}\left[Z_V(\Theta) - Z_V(\Theta+\pi)\right], & \text{if } k = 1, \\ 0, & \text{otherwise.} \end{cases} \tag{31}$$

$$\boldsymbol{C}_j^{k\,T}(\Theta)\boldsymbol{P}(t) = \begin{cases} \frac{u(t)}{2}Z_V'(\Theta) + \frac{u(t)}{2}Z_V'(\Theta+\pi), & \text{if } j = k = 1, \\ u(t)Z_V'(\Theta), & \text{if } j = k \text{ and } 2 \le j \le \mathrm{N}/2, \\ u(t)Z_V'(\Theta+\pi), & \text{if } j = k \text{ and } N/2+1 \le j \le \mathrm{N}-1, \\ 0, & \text{otherwise.} \end{cases} \tag{32}$$

4 Necessary conditions for stabilization of population oscillations using periodic input

Stabilization of a periodically forced oscillator can be achieved by satisfying conditions (16)–(19) which use the phase-amplitude reduction as a starting point (5). As shown below, many of these conditions are redundant, and ultimately, relatively few are necessary even for large oscillator populations. Additionally, using equations (25)–(32) from the previous section, these stabilization conditions can be written solely in terms of the phase response curves of the individual oscillators, the phase differences in steady state, and the unstable Floquet exponents. The stabilization conditions given below are valid in the limit that the magnitude of periodic input is small and do not contain any explicit information about the basins of attraction of stabilized solutions. Nevertheless, in numerical results presented in Sect. 5 these conditions provide a strong foundation from which to design inputs that modify the stability of periodic solutions as desired. Results presented in Sect. 5.1 investigate modifications to the resulting basins of attraction of stabilized orbits in response to periodic forcing.

As an important side note, previous work illustrated that for an identical and uncoupled population of oscillators, input applied when the derivative of the phase response curve is large can exponentially desynchronize the population-the results from Sect. 4.2 show this result also holds when weak coupling is explicitly included in the analysis.

4.1 Stabilization of splay state solutions

As mentioned earlier, the nonzero eigenvalues of (24) are good approximations to the Floquet exponents, κ_i, of the periodic orbit from (9). As shown in Wilson (2019b), when each κ_i is unique, stabilization can be achieved by designing a stimulus for which (16)–(18) and (20) are all satisfied. From (26), however, note that each $\boldsymbol{C}_i^i(\Theta)^T\boldsymbol{P}(t)$ is identical to leading order for all i so that $\nu_{i,i}$ from (20) are identical. With this information, condition (20) can be simplified to

$$\max_i(\mathrm{real}(\kappa_i)) + \mathrm{real}(\nu_{i,i}(H_0)) < 0. \tag{33}$$

Equation (33) states that focusing solely on the largest magnitude Floquet multiplier, all unstable modes of the splay state can be stabilized regardless of the number of oscillators. Furthermore, as can be seen from (25) and (26), $\frac{d}{d\Theta}\left(\boldsymbol{Z}^T(\Theta)\boldsymbol{P}(t)\right) = \boldsymbol{C}_i^i(\Theta)^T\boldsymbol{P}(t)$. Recalling the definition of $\nu_{i,i}$, this implies that condition (17) is already satisfied when (33) is satisfied. Taken together, only a subset of the requirements (16)–(18) and (20) must be satisfied to stabilize the splay state:

$$\begin{aligned}\rho(H_0) &= -\Delta\Omega,\\ \mu_i(H_0) &= 0 \quad \text{for } i = 1,\ldots,\beta,\\ \max_i(\text{real}(\kappa_i)) + \text{real}(\nu_{i,i}(H_0)) &= \kappa_1^{\text{targ}} < 0.\end{aligned} \tag{34}$$

Here, κ_1^{targ} is a target value of the real component of the largest magnitude Floquet multiplier for the periodically perturbed system. Using the approximations for the reduced equations from (22), (25), and (26), the stability conditions above can be approximated by

$$\begin{aligned}&\frac{1}{T_p}\int_0^{\text{Tp}}\left(\frac{u(t)}{N}\sum_{i=1}^{N}\left[Z_V\left(H_0+\frac{2(j-1)\pi}{N}+\Omega_p t\right)\right]\right)dt = -\Delta\Omega,\\ &\frac{1}{T_p}\int_0^{\text{Tp}}\left(u(t)\sum_{i=1}^{N}\left[w_k^i Z_V\left(H_0+\frac{2(j-1)\pi}{N}+\Omega_p t\right)\right]\right)dt = 0 \quad \text{for } k = 1,\ldots,\beta,\\ &\max_i(\text{real}(\kappa_i)) + \frac{1}{T_p}\int_0^{\text{Tp}}\left(\frac{u(t)}{N}\sum_{i=1}^{N}\left[Z_V'\left(H_0+\frac{2(j-1)\pi}{N}+\Omega_p t\right)\right]\right)dt = \kappa_1^{\text{targ}} < 0.\end{aligned} \tag{35}$$

4.2 Destabilization of synchronous solutions

For stable synchronous solutions (i.e., with $\eta_{i,j} = 0$ for all i and j), as shown in Appendix A.2, the associated matrix M from (24) has $N-1$ repeated nonzero eigenvalues with $\lambda_k = A/N$. Considering the conditions given in Sect. 2.3, a stable synchronous solution (i.e., with $\text{real}(\kappa_k) < 0$ for all k), can be destabilized provided there exists some H_0 for which

$$\rho(H_0) = -\Delta\Omega, \tag{36}$$

$$\mu_i(H_0) = 0 \quad \text{for } i = 1,\ldots,\beta, \tag{37}$$

$$\Lambda(D + E(H_0)) > 0. \tag{38}$$

Note that in contrast to (19), condition (38) requires some Floquet multiplier of the periodically forced synchronized orbit to be positive, thereby making it unstable. Condition (37) is guaranteed for the synchronous solution from any stimulus by (28) which states that isostable response curves are well approximated by zero. Additionally, using (29), one finds that $D + E(H_0)$ as defined in (15) is simply diagonal

$$D + E(H_0) = \begin{bmatrix}\kappa_1 + \nu_{1,1}(H_0) & & \\ & \ddots & \\ & & \kappa_{N-1} + \nu_{N-1,N-1}(H_0)\end{bmatrix}. \tag{39}$$

Furthermore, recall $\kappa_j \approx \lambda_j$ and that κ_j are identical for all j. Additionally, from (29), $\nu_{j,j}(H_0)$ is well approximated by $\frac{1}{T_p}\int_0^{T_p} Z_V'(H_0 + \Omega_p t)u(t)dt$ for all j. Therefore,

(38) can be satisfied provided $\kappa_1 + \nu_{1,1}(H_0) > 0$. To summarize, the synchronous state can be destabilized provided there exists some H_0 for which only two conditions are satisfied:

$$\begin{aligned} \rho(H_0) &= -\Delta\Omega, \\ \kappa_1 + \nu_{1,1}(H_0) &= \kappa_1^{\text{targ}} > 0. \end{aligned} \tag{40}$$

Additionally, from (27) and (29), in the limit that coupling is small, the above conditions are well approximated by

$$\begin{aligned} \frac{1}{T_p}\int_0^{\mathrm{T_p}} \left(u(t) Z_V\left(H_0 + \Omega_p t\right)\right) dt &= -\Delta\Omega, \\ \kappa_1 + \frac{1}{T_p}\int_0^{\mathrm{T_p}} \left(u(t) Z_V'\left(H_0 + \Omega_p t\right)\right) dt &= \kappa_1^{\text{targ}} > 0. \end{aligned} \tag{41}$$

In other words, Floquet multipliers of the coupled system of oscillators can be manipulated by applying a stimulus that is proportional to the derivative of the PRC of the individual oscillators. Previous work (Wilson and Moehlis 2014) yielded a related result through analysis of uncoupled, identical oscillators receiving the same inputs, i.e., that stimulation applied when the derivative of the PRC is large can exponentially desynchronize a pathologically synchronized population of neurons. The results here show that when coupling is explicitly included in the analysis, the derivative of the PRC still characterizes whether a stimulus will be effective at desynchronizing a pathologically synchronized population.

4.3 Stabilization of rotating block solutions

As will be shown here, the control objective of stabilizing a rotating block solution is a hybrid between stabilization of splay solutions and stabilization of synchronous solutions. Beginning with the stability requirements (16)–(19), suppose the goal is to stabilize the 2-block solution. Using (31), all but one isostable response curve is well approximated by zero, so that (18) can be satisfied by simply requiring $\mu_1(H_0) = 0$. In Appendix A.3 it is shown that the eigenvalues λ_2 through λ_{N-1} of the matrix M from (24) are identical so that κ_2 through κ_{N-1} are also identical to leading order. Considering $\boldsymbol{C}_j^k(\Theta)\boldsymbol{P}(t)$ from (32), the matrix $D + E(H_0)$ is diagonal with specific elements given by

$$\begin{aligned} &[D + E(H_0)]_{j,j} \\ &= \begin{cases} \kappa_1 + \frac{1}{T_p}\int_0^{T_p}\left[\frac{u(t)}{2} Z_V'(H_0 + \Omega_p t) + \frac{u(t)}{2} Z_V'(H_0 + \Omega_p t + \pi)\right] dt, & \text{if } j = 1, \\ \kappa_2 + \frac{1}{T_p}\int_0^{T_p}\left[u(t) Z_V'(H_0 + \Omega_p t)\right] dt, & \text{if } 2 \le j \le N/2, \\ \kappa_2 + \frac{1}{T_p}\int_0^{T_p}\left[u(t) Z_V'(H_0 + \Omega_p t + \pi)\right] dt, & \text{if } N/2 + 1 \le j \le N - 1, \end{cases} \end{aligned} \tag{42}$$

where $[D + E(H_0)]_{j,j}$ denotes the jth term on the diagonal of the matrix $D + E(H_0)$. Therefore, conditions (16)–(19) for the 2-block solution are satisfied provided the

simplified conditions below are satisfied for some H_0:

$$\begin{aligned}
\frac{1}{T_p}\int_0^{T_p}\left(\frac{u(t)}{2}\left[Z_V\left(H_0+\Omega_p t\right)+Z_V\left(H_0+\Omega_p t+\pi\right)\right]\right)dt &= -\Delta\Omega,\\
\frac{1}{T_p}\int_0^{T_p}\left(\frac{u(t)}{2}\left[Z_V\left(H_0+\Omega_p t\right)-Z_V\left(H_0+\Omega_p t+\pi\right)\right]\right)dt &= 0,\\
\kappa_1+\frac{1}{T_p}\int_0^{T_p}\left(\frac{u(t)}{2}\left[Z'_V\left(H_0+\Omega_p t\right)+Z'_V\left(H_0+\Omega_p t+\pi\right)\right]\right)dt &= \kappa_1^{\text{targ}}<0,\\
\kappa_2+\frac{1}{T_p}\int_0^{T_p}\left(u(t)\left[Z'_V\left(H_0+\Omega_p t\right)\right]\right)dt &= \kappa_2^{\text{targ}}<0,\\
\kappa_2+\frac{1}{T_p}\int_0^{T_p}\left(u(t)\left[Z'_V\left(H_0+\Omega_p t+\pi\right)\right]\right)dt &= \kappa_2^{\text{targ}}<0,
\end{aligned} \tag{43}$$

where, κ_1^{targ} and κ_2^{targ} are target values of the each Floquet multiplier under the application of the periodic stimulus. The first three conditions of (43) are identical to the stabilization conditions for the 2-oscillator splay stabilization. The remaining two conditions ensure that the rotating blocks themselves are stable. One can show that this general pattern persists for rotating block solutions with larger than 2 blocks by generalizing the arguments presented here and in Appendix A.3.

5 Numerical results

To illustrate the theoretical results presented above a population model of spiking thalamic neurons with synaptic coupling will be considered (Rubin and Terman 2004). Other forms of coupling [such as electrotonic coupling (Johnston and Wu 1995)] could also be considered provided the dynamical equations can be written in the same form as Eq. (3). The model equations are given by

$$\begin{aligned}
C\dot{V}_i &= -I_{\text{L}}(V_i)-I_{\text{Na}}(V_i,h_i)-I_{\text{K}}(V_i,h_i)-I_{\text{T}}(V_i,r_i)\\
&\quad +I_{\text{SM}}-\frac{g_{\text{syn}}}{N}\sum_{j=1}^{N}s_j(V_i-E_{\text{syn}})+u(t),\\
\dot{h}_i &= (h_\infty(V_i)-h_i)/\tau_h(V_i),\\
\dot{r}_i &= (r_\infty(V_i)-r_i)/\tau_r(V_i),\\
\dot{s}_i &= \frac{a(1-s)}{1+\exp(-(V_i-V_T)/\sigma_T)}-bs_i.
\end{aligned} \tag{44}$$

Here, N represents the number of neurons in the population, V_i, s_i, h_i, and r_i are the transmembrane voltage, synaptic variable, and two gating variables of neuron i, respectively, g_{syn} is a constant conductance that determines the coupling strength, $E_{\text{syn}} = -100$ mV is the reversal potential of the neurotransmitter so that the

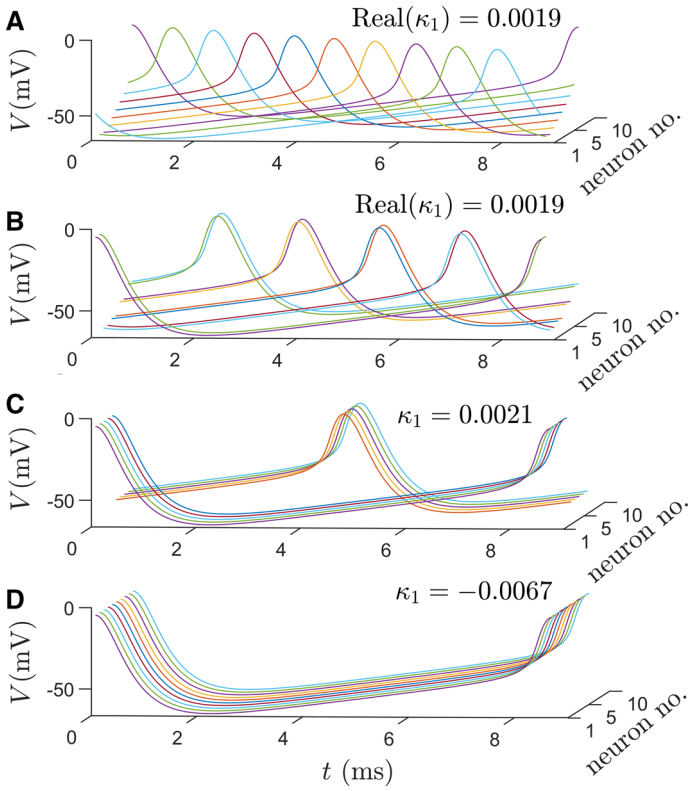

Fig. 2 Panel **A** shows the unstable splay orbit for $N = 10$ neurons. Unstable rotating block orbits with 5 and 2 blocks are shown in panels **B** and **C**, respectively. The stable synchronized state is shown in panel **D**. The rate of growth or decay of perturbations from these periodic orbits can be determined from the principal Floquet multiplier, κ_1

coupling is inhibitory, $u(t)$ is an injected current which is identical for all neurons, $C = 1\mu\text{F/cm}^2$ is the membrane capacitance, and I_{SM} is a baseline current taken to be 5 $\mu\text{A/cm}^2$. Specific parameters that determine the synaptic current are $a = 3$, $V_t = -20\,\text{mV}$, $\sigma_T = 0.8\,\text{mV}$, and $\beta = 0.2$. The reader is referred to Rubin and Terman (2004) for a full explanation of the remaining functions that determine the ionic currents and the behavior of the gating variables.

For this neural model, taking $g_{\text{syn}} = 0.015\,\text{mS/cm}^2$ and $u(t) = 0$ the synchronized state is stable for all choices of N, with unstable periodic orbits corresponding to both the rotating block and splay states. Figure 2 shows these different periodic orbits for $N = 10$ neurons with unstable splay and rotating block orbits shown in panels A–C and the synchronized state shown in panel D. Each of the splay and rotating block states has similar principal Floquet exponent with $\text{Real}(\kappa_1) \approx 0.002$ (recall that κ_1 is the Floquet exponent with the largest real component that determines the stability of the periodic orbit).

For each of the periodic orbits shown in Fig. 2, the population phase response curve from the reduction (6) is computed numerically and shown in the top panels of Fig. 3.

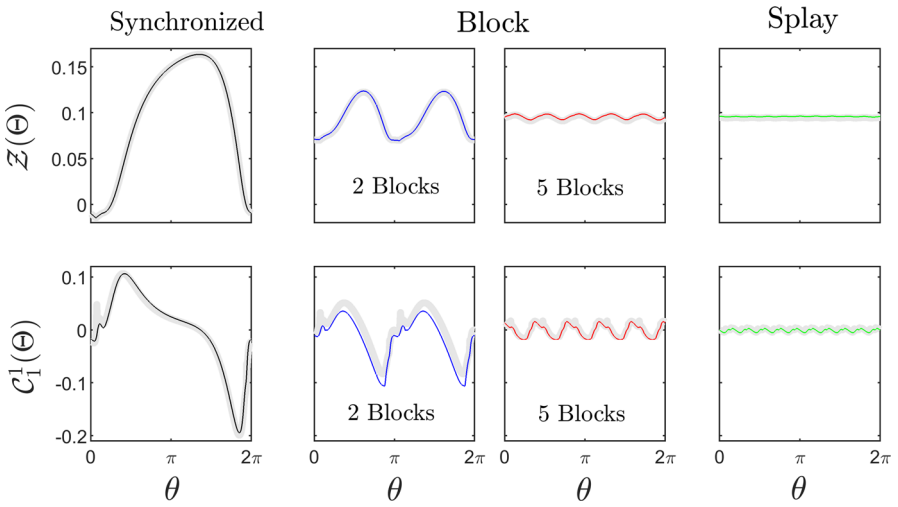

Fig. 3 Top and bottom panels show $\mathcal{Z}(\Theta)$ and $\mathcal{C}_1^1(\Theta)$ for each periodic orbit from Fig. 2. Thin lines are computed numerically and the gray lines are approximations based solely on the phase response curves $Z_V(\theta)$ of the individual neurons

Additionally, the function $\mathcal{C}_1^1(\Theta)$ (which is used to design stimuli to modify stability of these orbits) is shown in the bottom panels. Thin lines show curves calculated numerically using methods described in Wilson (2019a), and thick, gray lines show approximations based on the phase response curves of a single neuron $Z_V(\theta)$ using relationships derived in Sect. 3 that are valid in the limit of small coupling. The curves calculated directly from (44) are nearly identical to those approximated from the PRCs of the individual neurons.

In Fig. 3, notice that for periodic orbits containing more blocks, the magnitude of $\mathcal{C}_1^1(\Theta)$ becomes smaller and smaller. Recalling that $\mathcal{C}_1^1(\Theta)u(t) \approx \boldsymbol{C}_1^{1\,T}(\Theta)\boldsymbol{P}(t)$, intuitively this occurs because at larger values of N the relationship (26) can be written as $\boldsymbol{C}_j^{j\,T}(\Theta)\boldsymbol{P}(t) \approx \frac{u(t)}{N}\sum_{i=1}^{N}\left[Z_V'\left(\Theta+\frac{2(j-1)\pi}{N}\right)\right] \approx \frac{u(t)}{2\pi}\int_0^{2\pi} Z_V'(\Theta)d\Theta = 0$.

In Fig. 4 stabilization of splay states is investigated for the population in (44) with $g_{\text{syn}} = 0.03\,\text{mS/cm}^2$ for various numbers of neurons. Using methods described in Appendix B, periodic stimuli are designed to stabilize the unstable splay states by satisfying the stabilization conditions (34). Panels A and B show the resulting optimal periodic stimuli (black lines) for stabilizing the splay state with 2 (resp., 5) neurons when choosing the target value of κ_1 to be -0.005. For reference, sinusoidal stimuli with period $T/2$ and $T/5$ are shown as dashed gray lines. The sinusoidal stimuli for stabilizing the splay states are very close to optimal. Panel C shows how the principal Floquet multipliers of the splay states change when sinusoidal perturbation with an appropriate frequency is applied to (44) for different values of N. Larger magnitude sinusoidal perturbations are required to stabilize the splay state as N becomes larger. To explain this behavior, notice that the magnitude of $\mathcal{C}_1^1(\Theta)$ shrinks as N becomes larger. Recalling that $\mathcal{C}_j^k(\Theta)u(t) \approx \boldsymbol{C}_j^{k\,T}(\Theta)\boldsymbol{P}(t)$, from the stabilization conditions

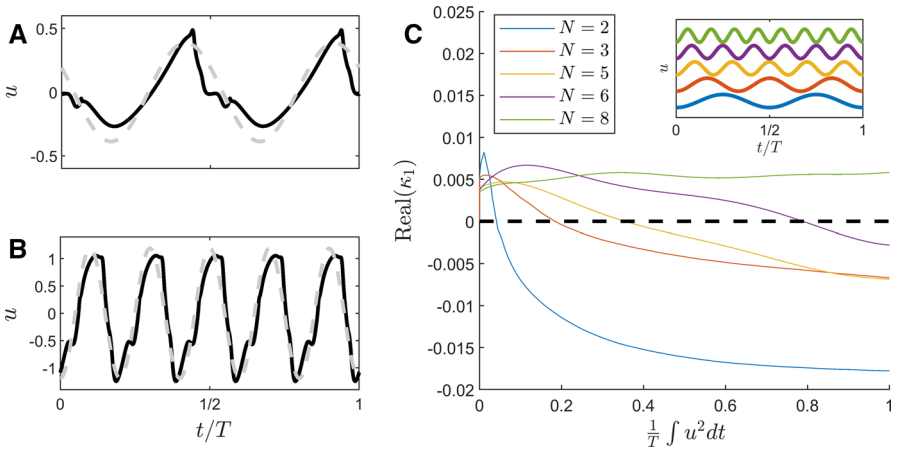

Fig. 4 Panels **A** and **B** show optimal periodic stimuli for stabilizing the splay states of (44) as black lines with $N = 2$ and $N = 5$ neurons, respectively. For each, the target Floquet multiplier is -0.005. Both stimuli are successful at stabilizing the splay states. For $N = 2$ (resp., 5) the actual Floquet multiplier is -0.0048 (resp., -0.0031) with an average energy usage of $\frac{1}{T}\int u^2 dt = 0.046$ (resp., 0.64). For reference, sinusoidal perturbations with period T/N are shown as gray dashed lines. In each case, they result in a Floquet exponent identical to the one obtained using the optimal stimulus but use more energy; for these stimuli, $\frac{1}{T}\int u^2 dt = 0.075$ and 0.71 for $N = 2$ and 5, respectively. Panel **C** gives a plot of κ_1 for the unstable splay state for different values of N when sinusoidal perturbation with period T/N is applied. As expected from the numerical calculations of $C_1^1(\Theta)$ and corresponding analytical results, more energy is required to stabilize the splay state as N increases (color figure online)

from Sect. 4, smaller values of $\boldsymbol{C}_j^j(\Theta)$ will require larger magnitude perturbations $u(t)$ to yield comparable values of $v_{i,i}$. The values of $v_{i,i}$ determine the Floquet exponents of periodically perturbed solutions and because the splay and rotating block solutions have comparable Floquet exponents it is expected to require larger magnitude external input to stabilize periodic orbits with more blocks. For this particular example, when $N = 8$, the splay state cannot be stabilized for any magnitude of perturbation. At this point, the magnitude of the perturbations required becomes large enough invalidate the phase-amplitude reduction (5).

5.1 Open loop desynchronization with negligible noise and heterogeneity

The previous section investigated stabilizing splay state solutions with no consideration of their basin of attraction. Here, the problem of destabilizing a synchronous solution in favor of a splay state solution will be considered. To accomplish this goal, additional factors will need to be considered when the initial conditions are near the stable synchronized state. Related control objectives were considered in Monga and Moehlis (2019) and Matchen and Moehlis (2018) with the goal of splitting a synchronized population into multiple clusters using feedback. Here, however, this objective is completed without state feedback. Clustering of uncoupled oscillators subject to noise was also considered in Nakao et al. (2007).

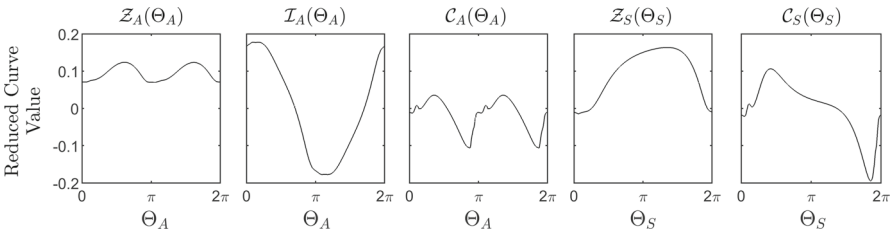

Fig. 5 Each of the reduced curves from (45) for the periodic orbits of (44) corresponding to the synchronous and splay states are shown in the panels above. All of these curves must be used to satisfy the conditions (46) to appropriately modify the stability of the asynchronous and synchronous state in response to periodic stimulation

To begin, consider $N = 2$ neurons with a stable synchronized solution and an unstable splay state. Each of these periodic solutions has reduced equations of the form (6)

$$\begin{aligned}
\dot{\Theta}_S &= \Omega_S + \mathcal{Z}_S(\Theta_S)u(t) + \mathcal{B}_S(\Theta_S)\psi_S u(t),\\
\dot{\psi}_S &= \kappa_S \mathcal{I}_S(\Theta_S)u(t) + \mathcal{C}_S(\Theta_S)\psi_S u(t),\\
\dot{\Theta}_A &= \Omega_A + \mathcal{Z}_A(\Theta_A)u(t) + \mathcal{B}_A(\Theta_A)\psi_A u(t),\\
\dot{\psi}_A &= \kappa_A \mathcal{I}_A(\Theta_A)u(t) + \mathcal{C}_A(\Theta_A)\psi_A u(t).
\end{aligned} \tag{45}$$

In the above equation the synchronized and splay (asynchronous) states have different reduced equations and coordinates with the subscript S and A denote the reduced terms associated with the synchronized and splay states, respectively. Additionally, because $N = 2$, there is only one isostable coordinate for each periodic orbit and the numerical subscripts and superscripts have been dropped for notational convenience. The curves from (45) using the model (44) are calculated numerically using $g_{\text{syn}} = 0.015\,\text{mS/cm}^2$ and shown in Fig. 5. For this choice of parameters, $\kappa_A = 0.0021$ and $-\kappa_S = 0.0067$ indicating that the splay and synchronized states are unstable and stable, respectively.

The goal here will be to determine a periodic stimulus that simultaneously destabilizes the synchronous solution and stabilizes the splay state. This can be achieved by designing a single T_p-periodic stimulus (with natural frequency $\Omega_p = 2\pi/T_p$) that satisfies both (34) and (40) such that there exists some H_1 and H_2 for which

$$\begin{aligned}
\rho^A(H_1) &= -(\Omega_A - \Omega_p),\\
\mu^A(H_1) &= 0,\\
\text{real}(\kappa_A) + \nu^A(H_1) &= \kappa_A^{\text{targ}} < 0,\\
\rho^S(H_2) &= -(\Omega_S - \Omega_p),\\
\kappa_S + \nu^S(H_2) &= \kappa_S^{\text{targ}} > 0.
\end{aligned} \tag{46}$$

In the above equation, $\rho^X(H) = \frac{1}{T_p}\int_0^{T_p} \mathcal{Z}_X(H + \Omega_p t)u(t)dt$, $\nu^X(H) = \frac{1}{T_p}\int_0^{T_p} \mathcal{C}_X^T(H + \Omega_p t)u(t)dt$, and $\mu^A(H) = \frac{1}{T_p}\int_0^{T_p} \mathcal{I}_A(H + \Omega_p t)u(t)dt$ with $X = A$

and S. As illustrated in Appendix B, conditions (46) can be written in the general form (B1) and optimal solutions can be found for arbitrary choices of κ_S^{targ} and κ_A^{targ}. Additionally, Ω_p is taken to be identical to Ω_A. This procedure is implemented using the numerically calculated curves from Fig. 5 with resulting stimuli shown in panels B and D of Fig. 6 for two different values of κ_A^{targ} and κ_S^{targ} with H_1 and H_2 chosen to be $5\pi/3$ and 0, respectively. To investigate the desynchronizing ability of these resulting stimuli the preliminary reduction (3) will be analyzed in a rotating and averaged reference frame. Starting from the equation describing the reduced and coupled oscillators (3) and letting $r_i = \theta_i - \Omega_p t$ for $i = 1, 2$ one finds

$$\begin{aligned}
\dot{r}_1 &= \omega - \Omega_p + Z_V(r_1 + \Omega_p t)\Big[u(t) + \frac{g_{\text{syn}}}{2}\big(s(r_2 + \Omega_p t) - s(r_1 + \Omega_p t)\big)\big(V(r_1 \\
&\quad + \Omega_p t) - E_{\text{syn}}\big)\Big], \\
\dot{r}_2 &= \omega - \Omega_p + Z_V(r_2 + \Omega_p t)\Big[u(t) + \frac{g_{\text{syn}}}{2}\big(s(r_1 + \Omega_p t) - s(r_2 + \Omega_p t)\big)\big(V(r_2 \\
&\quad + \Omega_p t) - E_{\text{syn}}\big)\Big].
\end{aligned} \tag{47}$$

Provided $\Omega_p - \omega$ is order ϵ, and assuming the influence of synaptic coupling is also an order ϵ term, (47) is periodic and in the general form $\dot{\boldsymbol{y}} = \epsilon Q(\boldsymbol{y}, t)$ so that the method of averaging can be employed (Sanders et al. 2007; Guckenheimer and Holmes 1983) to approximate (47) by

$$\begin{aligned}
\dot{R}_1 &= \omega - \Omega_p + f_{\text{av}}(R_1, R_2), \\
\dot{R}_2 &= \omega - \Omega_p + f_{\text{av}}(R_2, R_1),
\end{aligned} \tag{48}$$

where $f_{\text{av}}(x, y) = \frac{1}{T_p}\int_0^{T_p} Z_V(x+\Omega_p t)\big[u(t)+\frac{g_{\text{syn}}}{2}\big(s(y+\Omega_p t)-s(x+\Omega_p t)\big)\big(V(x+\Omega_p t) - E_{\text{syn}}\big)\big]dt$. Panels A and C of Fig. 6 show individual trajectories of (48) with initial conditions starting near the fixed point at $R_1 = R_2 = 0$ using the stimuli from panels B and D, respectively. The initial conditions for these trajectories are taken from a circle of radius 0.05 centered at the origin. While both stimuli destabilize the the fixed point corresponding to synchronous solutions, the basins of attraction of each the splay states are significantly different. For instance, in panel A, a very small proportion of initial conditions end up in the splay state, with the remainder shifting to a different synchronized fixed point. This is because κ_S^{targ} is chosen to be relatively small and initial conditions are pushed more strongly along unstable eigendirections towards fixed points of synchronized states. Conversely, many more initial conditions end up in the splay state in simulations from panel C. In these simulations, κ_S^{targ} is much larger so that initial differences in phase are amplified more rapidly resulting in a larger basin of attraction of the splay state.

Finally, this general strategy is used to design a periodic stimulus to split a population of synchronized neurons into separate clusters. This is accomplished by finding a stimulus to satisfy the conditions (46) optimally using the methods from Appendix B for two neurons from (44) with $g_{\text{syn}} = 0.03\,\text{mS/cm}^2$. Recalling the results from Fig. 6,

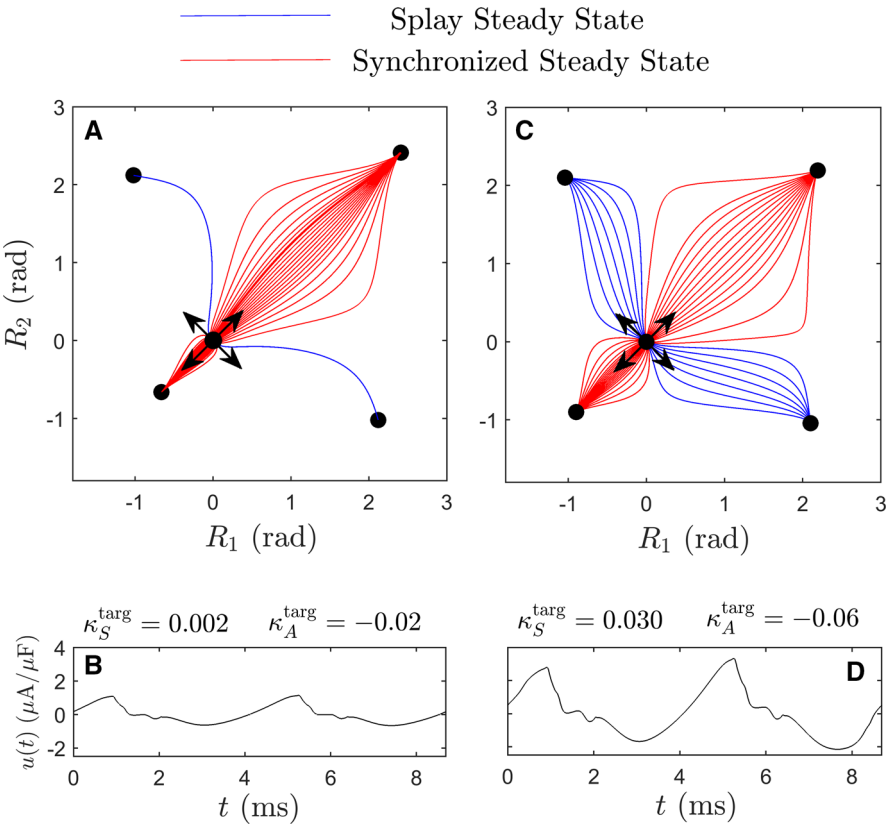

Fig. 6 Panel **A** (resp., **C**), shows individual trajectories of (48) under the application of the periodic stimulus from panel **B** (resp., **D**). Initial conditions are chosen near the unstable fixed point at $R_1 = R_2 = 0$. In panels **A** and **B**, black dots indicate fixed points of (48). Stimuli in panels **B** and **D** are designed to destabilize the fixed point at the origin and stabilize the splay state. For larger values of κ_S^{targ} (which determines the Floquet exponent of the synchronous state) the basin of attraction of the splay state is increased (color figure online)

the basin of attraction of the splay state is increased as κ_S^{targ} (resp., κ_A^{targ}) is increased (resp., decreased). The values of κ_A^{targ} and κ_S^{targ} chosen for the optimization are -0.06 and 0.02, respectively, with $H_1 = 5\pi/3$ and $H_2 = 0$.

The resulting stimuli is applied to a population of 1000 identical neurons from (44). In these simulations, independent and identically distributed zero mean white noise with intensity 0.02 is added to the voltage variable of each neuron. This noise intensity is small relative to the coupling strength so that in steady state with $u = 0$, synchronous behavior results with only a small difference between the phases of each neuron. In Fig. 7, the optimal periodic stimulus is turned on at $t = 0$ ms and shown in Panel B. Panel A shows traces of the transmembrane voltage of individual neurons along with the average voltage in black. Provided the stimulus is turned on close to the moment that the synchronized neurons spike, they will gradually be separated until two nearly identical clusters form in steady state. As an additional tool to evaluate synchronization, the Kuramoto order parameter (Kuramoto 1984) defined according to

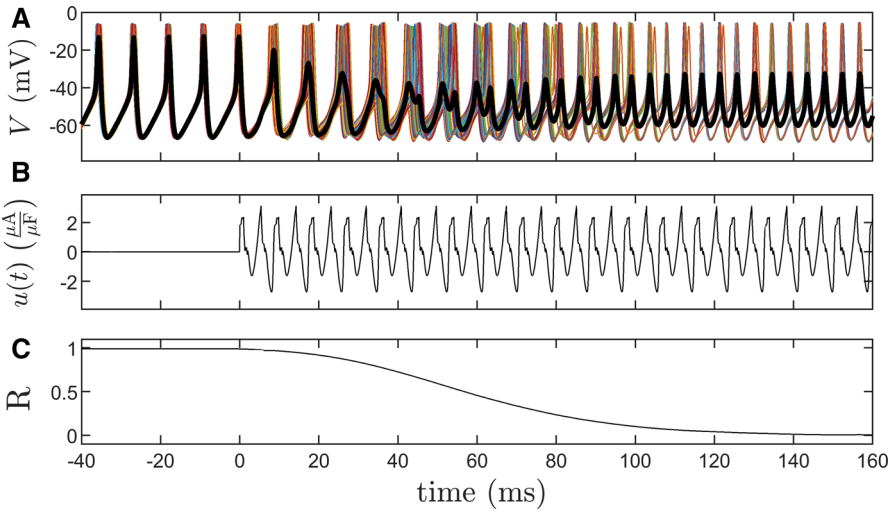

Fig. 7 Simulations of (44) with periodic control applied to both destabilize the synchronized state and stabilize the two-block rotating solution. Colored lines in panel **A** show individual voltage traces with the black line showing the average voltage of the population. The periodic stimulation is turned on at $t = 0$ ms and maintained throughout the rest of the simulation. As illustrated by the order parameter in Panel **C**, two separate clusters emerge in steady state after approximately 100 ms (color figure online)

$$R = \frac{1}{N}\left|\sum_{k=1}^{N} e^{i\theta_k}\right|, \tag{49}$$

is shown in panel C for this simulation. While the order parameter is not a perfect measure of synchronization, it does give a good sense of how well the control objective is achieved with values near 1 corresponding to the synchronized state and values near 0 corresponding to the rotating block solution.

The strategies illustrated above indicate that the methods presented in Sect. 4 can be applied to modify the stability of synchronized, splay, and rotating block states simultaneously. Such strategies are most useful when noise and heterogeneity is negligible relative to the size of the coupling so that the synchronous state needs to be actively desynchronized. As will be shown in the sections to follow, when noise and heterogeneity are larger, simply designing stimuli to stabilize the underlying splay states can be sufficient to disrupt synchronous behavior.

5.2 Desynchronization with non-negligible noise and heterogeneity

Here, Equation (44) will now be considered when incorporating noise and heterogeneity that cannot be neglected. Each simulation shown below contains 1000 neurons, each with the baseline current, I_{SM}, of the kth neuron equal to $4.95 + 0.0001k$ with resulting natural periods ranging from 8.34–8.45 ms in the absence of synaptic coupling. Additionally, all neurons have independent and identically distributed zero mean white noise with intensity 0.05 is added to the voltage variable and g_{syn} is taken to be

$0.03\,\mathrm{mS/cm^2}$. All other parameters are identical to those given as part of the definition of (44).

Using the conditions from (34) for stabilizing splay states, optimal stimuli are designed for various values of κ_1^{targ}. Panel A of Fig. 8 shows optimal stimuli calculated with $\kappa_1^{\text{targ}} = -0.045$ for different values of N. As mentioned earlier, the magnitude of $C_1^1(\Theta)$ shrinks as N increases which results in an increase in the magnitude of u. In panels C-E, a periodic stimulus is designed using $\kappa_1^{\text{targ}} = -0.04$ and $N = 3$ and applied to the neural population (44). Panel C shows the distribution directly before and after the stimulus is turned on at $t = 0$ ms. As time progresses, the population tends to split into three distinct clusters, with steady state behavior shown in panel D. Panel E gives the order parameter for this simulation, calculated according to (49) indicating that the population is split into 3 nearly identical clusters approximately 700 ms after the stimulus is turned on. Optimal stimuli are calculated for many different values of N and κ_1^{targ}. Starting from a synchronized state at $t = 0$ ms, these stimuli are applied for 3500 ms, which is long enough for transient behavior to die out. The steady state order parameter R_{ss} is calculated for each trial by averaging the order parameter R over the final 1000 ms. Results are shown in panel B. In these simulations, the periodic stimuli are designed solely to stabilize the splay states, with no consideration for destabilizing the synchronized state. Nevertheless, once κ_1^{targ} becomes large enough, separation of the neurons into different clusters starts to occur for simulations with $N = 3$, 4, and 5. Additionally, the initial time that the stimulation is turned on does not qualitatively influence the steady state behavior. A related problem was considered in Wilson and Moehlis (2015), where it was shown high frequency stimuli could reliably and predictably separate uncoupled neurons into multiple equal clusters in the presence of noise using an argument based on deterministic maps.

Finally to investigate whether the stabilization of the underlying splay states is important in desynchronization observed in Fig. 8, qualitatively different stimuli are applied to (44). Parameters are identical to those used in simulations shown in Fig. 8 and the resulting population behavior is considered. Here three types of stimuli are used. First, stimuli which optimally stabilize the splay state for $N = 3$ are considered, with an example for $\kappa_1^{\text{targ}} = -0.04$ shown in blue in panel A of Fig. 9. Additionally, sinusoidal stimuli of the form $u(t) = c \sin\left(\frac{2\pi t}{T_{\text{sp}}/3.5}\right)$ are considered, where T_{sp} is the natural frequency of the unstable splay state for $N = 3$ and c is a constant. This form of stimulus is chosen to yield a mismatch between the natural frequency of the splay state and the the stimulation so that no locking, and hence, no stabilization of the splay state will occur. The final stimulus takes $u(t)$ to be changing randomly at each time step Δt according to

$$u(t + \Delta t) = \begin{cases} -u(t), & \text{if } r < \frac{6\Delta t}{T_{\text{sp}}}, \\ u(t), & \text{otherwise.} \end{cases} \tag{50}$$

where r is a random number between 0 and 1 chosen independently at each time step from a uniform distribution. The particular choice of (50) ensures that on average, there will be 6 expected transitions between positive and negative values every T_{sp}

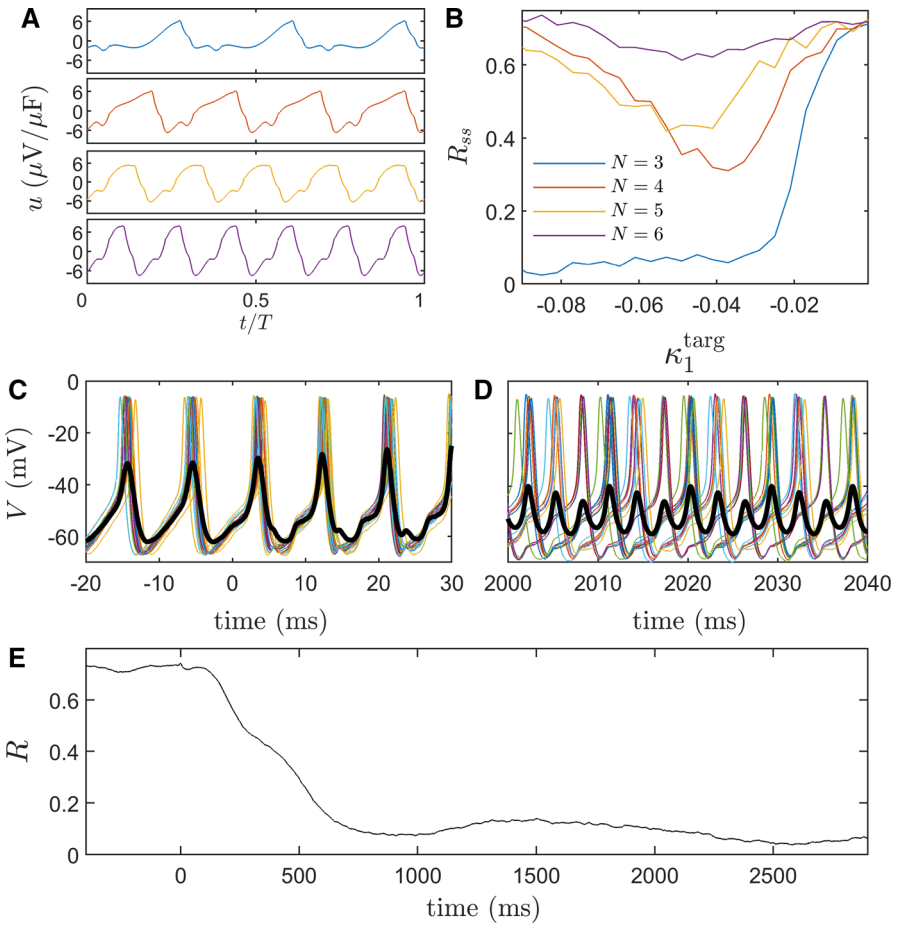

Fig. 8 In panel A, optimal stimuli designed to stabilize the splay state of (44) with a resulting $\kappa_1^{\text{targ}} = -0.045$ are shown for various values of N. Panels C-E show simulation results using a stimulus for which $\kappa_1^{\text{targ}} = -0.04$ and $N = 3$. Here, stimulation is first applied starting at $t = 0$ ms. The neurons are initially synchronized, but gradually separate into multiple, nearly equal clusters. The order parameter in panel E shows that the separation of the neurons happens gradually over the course of approximately 700 ms. Panel B shows the steady state order parameter in simulations with various choices of N and κ_1^{targ} (color figure online)

milliseconds just like for the optimal stimulus. Panel A of Fig. 9 shows examples of each of these stimuli, each with an identical energy consumption calculated according to $\frac{1}{T}\int_0^T u^2 dt$. The stimuli from panel A are applied to (44) with the resulting Kuramoto order parameter given in panel B for one representative trial. While the stimulus designed to optimally stabilize the splay state does indeed separate the population into separate clusters, the sinusoidal perturbation has little effect on the order parameter. The random perturbation chosen according to (50) is able to transiently reduce the order parameter, but on average the resulting population is more synchronized than it is without this random input. Panels C through E of Fig. 9 give traces of 25 representative

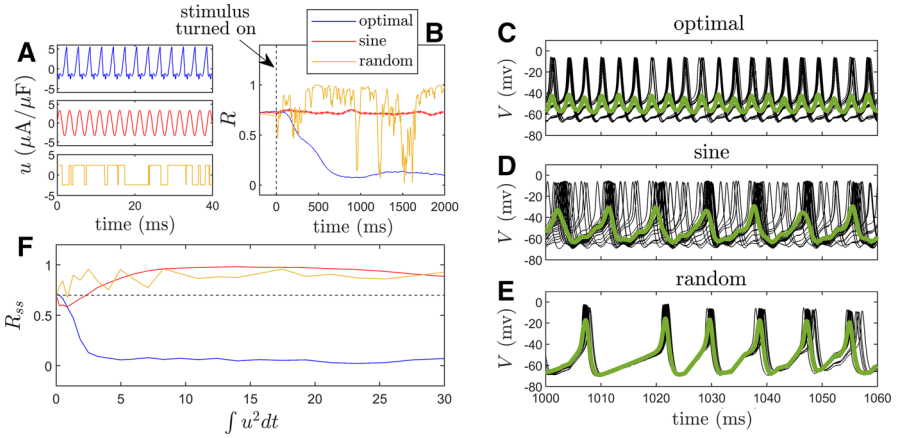

Fig. 9 Panel **A** shows three different types of stimuli considered in simulations of (44). The blue stimulus is determined by optimally stabilizing the splay state for $N = 3$. The red stimulus is sinusoidal and the yellow stimulus is randomly generated according to (50). Panel **B** shows the Kuramoto order parameter plotted for each stimulus type from panel **A**. Panels **C** through **E** show voltages traces of representative neurons (black lines) from the simulations from panel **B**. The green lines show the average transmembrane voltage for the population. In panel **F**, optimal, sinusoidal, and random perturbations with different energy consumption are applied and plotted against the steady state order parameter (color figure online)

neurons from the simulations from panel B. Three distinct clusters emerge under the application of the optimal input while the sinusoidal stimulation yields a distributions with a single cluster. In general, the random input has a synchronizing influence on the distribution, however, sometimes this random input does result in transient desynchronization.

Panel F of Fig. 9 gives a comparison of energy consumption versus R_{ss}, the steady state order parameter taken as the average value of R over the final 1000 ms (after transient behavior is allowed to die out). For the optimal stimuli, energy consumption is controlled through the choice of κ_1^{targ} when solving the optimization problem. For the other stimuli, energy consumption is controlled by changing the magnitude of the applied stimulus. At almost all values of power consumption, the sinusoidal and random perturbations yield stronger synchronization. Despite the fact that none of the other stable periodic solutions of (44) are considered in the design of the optimal stimuli from Figs. 8 and 9 neurons tends to end up in rotating block states when external perturbation designed to stabilize the corresponding splay states is applied.

6 Discussion and conclusion

This work investigates the ability of open-loop periodic stimulation to manipulate the stability of synchronized, splay, and rotating block solutions in populations of periodically firing neurons. Using Floquet theory as a backdrop for this analysis, stable and unstable modes of periodic solutions of coupled oscillator models are identified. Subsequent analysis of the nonlinear phase-amplitude reduced dynamics yields a strategy

to design optimal stimuli to modify the stability of these modes in a weakly perturbed setting. Surprisingly, in the weakly coupled limit, the phase response curve and natural frequency of individual neurons are the only information required to design appropriate stimuli to stabilize the splay states. Additionally, this strategy can be used to design stimuli that destabilize a synchronized solution in favor of a rotating block solution.

When the noise is small and oscillators are homogeneous, desychronization can only be achieved by designing a stimulus which actively destabilizes the synchronized solution while simultaneously stabilizing a chosen rotating block solution. This strategy was effective when attempting to split a synchronized population of neurons into two rotating blocks, but was difficult to implement in the full model (44) when attempting to separate into three or more rotating blocks. If desynchronization is the ultimate goal of periodic forcing, separation into more blocks would ultimately be better. For example, even though the order parameter drops close to zero after the two-block solution is stabilized in Fig. 7, the individual populations are still synchronized. Separation into more blocks (with fewer neurons in each block) would reduce the overall level of coherence. In a low noise and low heterogeneity setting it may be possible to separate a population into a larger number of rotating blocks in stages, for instance, by first splitting a population into two blocks, and then using a second stimulus to perform a secondary splitting. This will be the subject of future work.

While the design strategy presented here does not explicitly take into account noise or heterogeneity in the system parameters, numerical simulations reveal that these features tend to aid in the transition from a synchronized solution to a rotating block solution. Additionally, when stimulation was applied with a mismatch between the splay state natural frequency and the stimulation frequency, synchronization was enhanced in numerical simulations. The results presented here are consistent with the clinically observed frequency dependent efficacy of deep brain stimulation. While DBS can be effective as a treatment for Parkinson's disease when applied at a wide range of frequencies ranging from 70 to 1000 Hz (Moro et al. 2002; Benabid et al. 1991), most patients respond better to certain combinations of frequencies and stimulation intensities. This necessitates a time-intensive tuning process that generally culminates in a therapeutic range of about 130–180 Hz (Volkmann et al. 2002; Kuncel and Grill 2004). It may be the case that the particular frequency and stimulation combinations that are effective at treating DBS are those that stabilize one of the rotating block states for a population of neurons resulting in a less synchronous state. If this is the case, the results presented in this work suggest that higher frequency DBS would take larger magnitude stimulation to be effective since higher frequencies correspond to more rotating blocks.

The results of this study have numerous limitations. Foremost, the computational neurons considered here are relatively simple. Each neuron is modeled as a single compartment with no spatial component. Additionally, each neuron receives direct charge injection which is not clinically possible. When DBS is applied in a clinical setting, there is a complicated relationship between the electric field generated by DBS, the spatial geometry of each neuron, and the activation of the soma, axons and dendrites (Anderson et al. 2018; McIntyre et al. 2004). In order to fully understand the effect of DBS on a population of neurons, these spatial features would need to be taken into account. Additionally, the results here only consider the behavior of a

single population of pathologically synchronized neurons. In reality, the symptoms of DBS result from interactions within the basal ganglia-cortical loop and the impacts of desynchronization on the components of this circuit have not been considered. Furthermore, the analytical derivations in this work do not include heterogeneity in the parameters of each neuron or in the effective perturbation felt by each neuron. While including heterogeneity in the neural parameters does not change the qualitative behavior of these simulations, it would be of interest to extend these analytical results to explicitly account for heterogeneity in the model. Finally, while this study only considers the behavior of periodically firing neurons, there is evidence that correlated neural bursting may be a contributing factor to Parkinson's disease (Hahn et al. 2008; Ammari et al. 2011). Each of these considerations would need to be addressed before the methods presented here could be used to inform design of DBS waveforms for Parkinson's disease treatment.

Results presented here suggest the possibility of designing periodic, open-loop stimulation that can destabilize a synchronized population of oscillators in favor of a splay or rotating block state. Nonfeedback methods like the one presented here are particularly important because real-time feedback control on the time scale of individual neural spikes is not yet possible in a clinical setting. These results represent a starting point which could ultimately aid in the design of more efficient DBS waveforms for the treatment of Parkinson's disease. Related results were obtained in Wilson and Moehlis (2015), where it was shown that a noisy, uncoupled, and large population of oscillators was guaranteed to separate into nearly equal clusters when stimulation was applied at certain frequencies. The results in this work were derived for coupled and finite, but noiseless populations of neural oscillators. While the methods presented here can be used to separate a population of synchronized neurons into multiple rotating blocks, numerical results suggest that this task can be aided when noise and heterogeneity are considered. It would be of interest to extend these results to explicitly include noise which could, for instance, be accomplished through the analysis of the Fokker-Planck equation (Gardiner 2004) in the limit as the number of neurons approaches infinity to understand this observed behavior greater detail.

Acknowledgements Funding was provided by National Science Foundation (Grant No. CMMI-1933583).

Appendix A Derivation of simplified response curves for population oscillations

In this Appendix, full derivations for the simplified reduced order equations from Sect. 3 are presented. To begin, Eq. (3) from the main text will be analyzed when $u(t) = 0$. Consider a periodic solution $\theta_k^{\text{per}}(t)$ of (3) for which $\theta_k^{\text{per}}(t) = \theta_k^{\text{per}}(t + T)$ for some $T = 2\pi/\Omega$ for all k. For an identical population of oscillators, many of these solutions are guaranteed to exist (e.g., splay state, rotating block, synchronized solutions), however, not all of these solutions will be stable (Ashwin and Swift 1992; Brown et al. 2004). For the remainder of of this derivation, assume that the state is close to one of these periodic solutions. Asymptotic expansion about such a periodic solution yields to leading order

$$\dot{\theta}_i = \omega + \frac{1}{N} Z_V(\theta_i^{\text{per}}) \sum_{j=1}^{N} f(\theta_i^{\text{per}}, \theta_j^{\text{per}}) + \frac{1}{N} Z_V'(\theta_i^{\text{per}}) \sum_{j=1}^{N} f(\theta_i^{\text{per}}, \theta_j^{\text{per}}) \Delta\theta_i + \frac{1}{N} Z_V(\theta_i^{\text{per}}) \sum_{j=1}^{N} f_b(\theta_i^{\text{per}}, \theta_j^{\text{per}}) \Delta\theta_j + \frac{1}{N} Z_V(\theta_i^{\text{per}}) \sum_{j=1}^{N} f_a(\theta_i^{\text{per}}, \theta_j^{\text{per}}) \Delta\theta_i. \tag{A1}$$

Here, $\Delta\theta_k(t) \equiv \theta_k(t) - \theta_k^{\text{per}}(t)$ for all k, $f_b \equiv \partial f/\partial b$, $f_a \equiv \partial f/\partial a$ and $' \equiv d/d\theta$. Noting that since the periodic solution θ_i^{per} satisfies the relationship $\dot{\theta}_i^{\text{per}} = \omega + \frac{1}{N} Z_V(\theta_i^{\text{per}}) \sum_{j=1}^{N} f(\theta_i^{\text{per}}, \theta_i^{\text{per}})$, Eq. (A1) can be rewritten as

$$\Delta\dot{\theta}_i = \frac{1}{N} Z_V'(\theta_i^{\text{per}}) \sum_{j=1}^{N} f(\theta_i^{\text{per}}, \theta_j^{\text{per}}) \Delta\theta_i + \frac{1}{N} Z_V(\theta_i^{\text{per}}) \sum_{j=1}^{N} f_b(\theta_i^{\text{per}}, \theta_j^{\text{per}}) \Delta\theta_j + \frac{1}{N} Z_V(\theta_i^{\text{per}}) \sum_{j=1}^{N} f_a(\theta_i^{\text{per}}, \theta_j^{\text{per}}) \Delta\theta_i. \tag{A2}$$

By assuming that $f(\theta_i, \theta_j)$ is an order ϵ term where $0 < \epsilon \ll 1$ asymptotic expansion in powers of ϵ can be used to show that $\theta_i^{\text{per}}(t) = \theta_i^{\text{per}}(0) + \omega t + \mathcal{O}(\epsilon)$. Thus, $\theta_j^{\text{per}} = \theta_i^{\text{per}} + \eta_{i,j} + \mathcal{O}(\epsilon)$ where $\eta_{j,i}$ is a constant. Additionally, $f_a(a, b)$ and $f_b(a, b)$ are assumed to be order ϵ terms. Using this information, (A2) can be rewritten to leading order as

$$\Delta\dot{\theta}_i = \frac{1}{N} Z_V'(\alpha + \omega t) \sum_{j=1}^{N} f(\alpha + \omega t, \alpha + \omega t + \eta_{i,j}) \Delta\theta_i + \frac{1}{N} Z_V(\alpha + \omega t) \sum_{j=1}^{N} f_b(\alpha + \omega t, \alpha + \omega t + \eta_{i,j}) \Delta\theta_j + \frac{1}{N} Z_V(\alpha + \omega t) \sum_{j=1}^{N} f_a(\alpha + \omega t, \alpha + \omega t + \eta_{i,j}) \Delta\theta_i, \tag{A3}$$

where $\alpha \equiv \theta_i^{\text{per}}(0)$ and is defined for notational convenience. Notice that (A3) is T-periodic and in the general form $\dot{\boldsymbol{y}} = \epsilon Q(\boldsymbol{y}, t)$ so that the method of averaging (Sanders et al. 2007; Guckenheimer and Holmes 1983) can be employed, thereby approximating (A3) with a system of linear equations

$$\frac{d}{dt} \begin{bmatrix} \phi_1 \\ \phi_2 \\ \vdots \\ \phi_N \end{bmatrix} = \frac{1}{N} \begin{bmatrix} A_1 + B(0) & B(\eta_{1,2}) & \dots & B(\eta_{1,N}) \\ B(\eta_{2,1}) & A_2 + B(0) & \dots & B(\eta_{2,N}) \\ \vdots & & \ddots & \vdots \\ B(\eta_{N,1}) & B(\eta_{N,2}) & \dots & A_N + B(0) \end{bmatrix} \begin{bmatrix} \phi_1 \\ \phi_2 \\ \vdots \\ \phi_N \end{bmatrix}, \tag{A4}$$

where,

$$A_i \equiv \frac{1}{T}\int_0^T \left[Z_V'(\omega t) \sum_{j=1}^{N} f(\omega t, \omega t + \eta_{i,j}) + Z_V(\omega t) \sum_{j=1}^{N} f_a(\omega t, \omega t + \eta_{i,j}) \right] dt,$$
$$B(\eta_{i,j}) \equiv \frac{1}{T}\int_0^T \left[Z_V(\omega t) f_b(\omega t, \omega t + \eta_{i,j}) \right] dt. \tag{A5}$$

According to averaging theory (Sanders et al. 2007), ϕ_i is a close approximation to $\Delta\theta_i$. Additionally, fixed points of (A4) correspond to periodic solutions of (A3) with the same stability.

The averaged equation (A4) can be written as a linear time invariant system

$$\dot{\boldsymbol{\Phi}} = M\boldsymbol{\Phi}, \tag{A6}$$

where $\boldsymbol{\Phi} = [\phi_1 \ \ldots \ \phi_N]^T$. For such a system, notice that the sum of row i is

$$A_i + \sum_{j=1}^{N} B(\eta_{i,j}) = \frac{1}{\omega N T}\int_0^T \left(\sum_{j=1}^{N} \frac{d}{dt}\left[Z_V(\alpha + \omega t) f(\alpha + \omega t, \alpha + \omega t + \eta_{i,j}) \right] \right) dt$$
$$= 0, \tag{A7}$$

where equivalence in the first line can be shown by direct differentiation and subsequent manipulation of the right hand side and the second line follows because $Z(\theta_i) f(\theta_i, \theta_j)$ is 2π-periodic. Thus, the matrix M always has a zero eigenvalue with corresponding eigenvector $[1 \ \ldots \ 1]^T$.

The representation (A6) is particularly useful because the eigenvalues, λ_i, and corresponding left and right eigenvectors of M denoted by $\boldsymbol{w}_i$ and $\boldsymbol{v}_i$ characterize the behavior of solutions near the fixed point. Ultimately, this characterization will allow the terms of the reduced population Eq. (5) from the main text to be represented in terms of the reduction of the individual oscillators (2). To proceed, the solution of (A6) can be written as (Hespanha 2018)

$$\boldsymbol{\Phi}(t - t_0) = \sum_{j=1}^{N} \left[\boldsymbol{w}_j^T \boldsymbol{\Phi}(t - t_0) \boldsymbol{v}_i \exp(\lambda_j (t - t_0)) \right]. \tag{A8}$$

Recalling that ϕ_i is well approximated by $\Delta\theta_i$ and the definitions $\boldsymbol{x}(t) \equiv [\theta_1(t) \ \ldots \ \theta_N(t)]$ and $\boldsymbol{x}^\gamma \equiv [\theta_1^{\text{per}}(t) \ \ldots \ \theta_N^{\text{per}}(t)]$ one can write

$$\boldsymbol{x}(t - t_0) \approx \boldsymbol{x}^\gamma(t - t_0) + \sum_{j=1}^{N} \left[\boldsymbol{w}_j^T (\boldsymbol{x}(t - t_0) - \boldsymbol{x}^\gamma(t - t_0)) \boldsymbol{v}_i \exp(\lambda_j (t - t_0)) \right], \tag{A9}$$

Equation (A9) provides a good approximation for the behavior near the splay state solution. Note also that (A9) has a similar structure to (9), i.e., it is an approxima-

tion to the solution obtained from Floquet theory where the eigenvalues of the matrix M correspond directly to the Floquet exponents from (9). Considering the definition of the phase Θ used in (10) and (11), Eq. (A9) implies that to a good approximation, $\partial\Theta/\partial\boldsymbol{x}$ (i.e., $\boldsymbol{Z}(\Theta)$) is orthogonal to all $\boldsymbol{v}_k$ for which $\kappa_k \neq 0$. In other words, $\boldsymbol{Z}(\Theta)$ must be proportional to $\boldsymbol{w}_N$, defined to be the left eigenvector corresponding to $\lambda_N = 0$. Finally the phase response curve is subject to the normalizing condition $[\boldsymbol{Z}^T(\Theta(t))][\frac{d\boldsymbol{x}}{dt}|_{\boldsymbol{x}^\gamma(\Theta(t))}] = \Omega$ (cf. Wilson 2019b; Brown et al. 2004; Kuramoto 1984; Monga et al. 2019). This normalization stems from the fact that in the absence of input, $\frac{d\Theta}{dt} = \frac{d\Theta}{dx}\frac{dx}{dt} = \Omega$. From (3), $\frac{d\boldsymbol{x}}{dt}|_{\boldsymbol{x}^\gamma(\Theta(t))} = \omega\mathbf{1} + \mathcal{O}(\epsilon) = \Omega\mathbf{1} + \mathcal{O}(\epsilon)$ where $\mathbf{1}$ is an appropriately sized vector of ones. Therefore, $\boldsymbol{Z}(\Theta)$ is well approximated by $\frac{1}{\boldsymbol{w}_N^T\mathbf{1}}\boldsymbol{w}_N$. Finally, with the definition of $\boldsymbol{P}(t)$ from (4),

$$\boldsymbol{Z}^T(\Theta)\boldsymbol{P}(t) = \frac{u(t)}{\boldsymbol{w}_N^T\mathbf{1}}\sum_{j=1}^{N}\left[Z_V(\theta_j^{\text{per}}(\Theta))w_N^j\right] \tag{A10}$$

is a good approximation to the effective phase response curve from the perturbation $u(t)$ where w_N^j is the jth element of $\boldsymbol{w}_N$.

A similar strategy can also be used to determine an approximation of the functions $\boldsymbol{I}_j(\Theta)$ and $\boldsymbol{C}_j^k(\Theta)$. To do so, consider a small perturbation $\partial\boldsymbol{x}$ to a trajectory $\boldsymbol{x}(t)$ at time t_0. From the definition of isostable coordinates (12) and the approximate solution (A9), one can show that the resulting perturbation to the isostable coordinate ψ_k is well approximated by

$$\delta\psi_j = \boldsymbol{w}_j^T\delta\boldsymbol{x}. \tag{A11}$$

Additionally comparing (9) and (A9), $\boldsymbol{v}_i$ is a good approximation for $\boldsymbol{q}_i(\theta(t))$. Considering both (9) and (13), this implies

$$\boldsymbol{x}(t) \approx \boldsymbol{x}^\gamma(\theta) + \sum_{k=1}^{N-1}\psi_k\boldsymbol{v}_k. \tag{A12}$$

From (3), for a perturbation $u(t)$ lasting δt milliseconds

$$\begin{aligned}\delta\boldsymbol{x} &= \begin{bmatrix} Z_V(\theta_1^{\text{per}} + \sum_{k=1}^{N-1}(\psi_k v_k^1)) \\ \vdots \\ Z_V(\theta_N^{\text{per}} + \sum_{k=1}^{N-1}(\psi_k v_k^N))\end{bmatrix}u(t)\delta t \\ &= \begin{bmatrix} Z_V(\theta_1^{\text{per}}) + Z_V'(\theta_1^{\text{per}})\sum_{k=1}^{N-1}(\psi_k v_k^1) \\ \vdots \\ Z_V(\theta_N^{\text{per}}) + Z_V'(\theta_N^{\text{per}})\sum_{k=1}^{N-1}(\psi_k v_k^N),\end{bmatrix}u(t)\delta t.\end{aligned} \tag{A13}$$

Above, v_k^i denotes the ith element of the vector $\boldsymbol{v}_k$ and order ψ^2 terms have been neglected. Finally, combining (A11) and (A13)

$$\delta\psi_j = \sum_{i=1}^{N}\left[w_j^i Z_V(\theta_i^{\text{per}})\right]u(t)\delta t + \sum_{k=1}^{N-1}\left[\psi_k \sum_{i=1}^{N}\left[w_j^i v_k^i Z_V'(\theta_i^{\text{per}})\right]\right]u(t)\delta t. \tag{A14}$$

Directly comparing (A14) to the result of the change in isostable coordinate mandated by (5) from the same perturbation, one finds that

$$\begin{aligned}\boldsymbol{I}_j^T(\Theta)\boldsymbol{P}(t) &= \sum_{i=1}^{N}\left[w_j^i Z_V(\theta_i^{\text{per}}(\Theta))\right]u(t),\\ \boldsymbol{C}_j^{k\,T}(\Theta)\boldsymbol{P}(t) &= \sum_{i=1}^{N}\left[w_j^i v_k^i Z_V'(\theta_i^{\text{per}}(\Theta))\right]u(t).\end{aligned} \tag{A15}$$

A.1 Reduction of splay state solutions

One solution of general interest is the splay state, for which the phases of all oscillators are spaced equally. For such a solution, M from (A6) is a circulant matrix specified by the vector $\frac{1}{N}[A+B(0)\ \ B(2\pi/N)\ \ B(4\pi/N)\ \ \ldots\ \ B(2\pi(N-1)/N)]^T$. Note here that the index on A is dropped because the entries on the diagonal are all identical. In the previous section it was shown that $\boldsymbol{v}_N = \frac{1}{\sqrt{N}}[1\ \ \ldots\ \ 1]^T$ is an eigenvector of M with corresponding eigenvalue $\lambda_N = 0$. Because M is circulant, the remaining eigenvectors and eigenvalues are known exactly and are specified for $k = 1, \ldots, N-1$ by Kra and Simanca (2012)

$$\lambda_k = \frac{1}{N}\left[A + \sum_{j=0}^{N-1} B\,(2\pi\, j/N)\,\gamma_k^j\right], \tag{A16}$$

$$\boldsymbol{v}_k = \frac{1}{\sqrt{N}}[1\ \ \gamma_k\ \ \gamma_k^2\ \ \ldots\ \ \gamma_k^{N-1}]^T, \tag{A17}$$

where $\gamma_k = \exp\left(2\pi k\sqrt{-1}/N\right)$. The eigenvectors (A17) form an orthonormal basis (Kra and Simanca 2012), so that the left eigenvector $\boldsymbol{w}_k = \boldsymbol{v}_k^*$ where * denotes the complex conjugate.

The remaining eigenvalues can be approximated in the limit as N approaches infinity using (A16). To do so, first consider the value of A/N as N becomes large. Starting with (A5),

$$A/N = \frac{1}{NT}\int_0^T\left[Z_V'(\omega t)\sum_{j=1}^{N} f(\omega t, \omega t + \eta_{i,j}) + Z_V(\omega t)\sum_{j=1}^{N} f_a(\omega t, \omega t + \eta_{i,j})\right]dt$$

$$\begin{aligned}
&\approx \frac{1}{TN}\int_0^T N Z_V'(\omega t)\bar{f}(\omega t) + N Z_V(\omega t)\bar{f}'(\omega t)dt \\
&= \frac{1}{T\omega}\int_0^T \frac{d}{dt}\left[Z_V(\omega t)\bar{f}(\omega t)\right]dt \\
&= 0. \qquad \text{(A18)}
\end{aligned}$$

In the second line above, for large N, the relationship $\sum_{j=1}^{N} f(\theta, \theta + 2\pi j/N) \approx N\bar{f}(\theta)$ is used where $\bar{f}(\theta) \equiv \frac{1}{2\pi}\int_0^{2\pi} f(\theta, \theta + x)dx$. The last line follows from the fact that $Z(\omega t)\bar{f}(\omega t)$ is T-periodic. Thus, for large N, the eigenvalues are well approximated by

$$\begin{aligned}
\lambda_k &\approx \frac{1}{N}\sum_{j=0}^{N-1} B\left(\frac{2\pi j}{N}\right)\exp\left(\frac{2\pi k\sqrt{-1}}{N}\right) \\
&\approx \frac{1}{2\pi}\int_0^{2\pi}\left[B(\theta)\exp(\theta\sqrt{-1})\right]d\theta. \qquad \text{(A19)}
\end{aligned}$$

In other words, in the large N limit, the eigenvalues are well approximated by the Fourier coefficients of $B(\theta)$ and do not change significantly as N increases. Note that while (A19) is valid in the limit of large N, these eigenvalues can still be calculated directly from (A16) for any N.

For the splay state, the PRC can be simplified further from (A10). Recalling that the $\boldsymbol{v}_k$ from (A17) form an orthonormal basis, considering the left eigenvector associated with the zero eigenvalue $\boldsymbol{w}_N = \frac{1}{\sqrt{N}}\mathbf{1}$ one finds from (A10)

$$\begin{aligned}
\boldsymbol{Z}^T(\Theta)\boldsymbol{P}(t) &= \frac{u(t)}{N}\sum_{j=1}^{N}\left[Z_V(\theta_j^{\text{per}}(\Theta))\right] \\
&= \frac{u(t)}{N}\sum_{j=1}^{N}\left[Z_V\left(\Theta + \frac{2(j-1)\pi}{N}\right)\right]. \qquad \text{(A20)}
\end{aligned}$$

Above, the relationship $\theta_1^{\text{per}} = \Theta$ is used, with all other oscillators spaced equally around the ring. Additionally, noting that $w_j^i v_j^i = 1/N$ this offers the simplification to (A15)

$$\begin{aligned}
{\boldsymbol{C}_j^i}^T(\Theta)\boldsymbol{P}(t) &= \frac{u(t)}{N}\sum_{i=1}^{N}\left[Z_V'(\theta_i^{\text{per}}(\Theta))\right] \\
&= \frac{u(t)}{N}\sum_{i=1}^{N}\left[Z_V'\left(\Theta + \frac{2(j-1)\pi}{N}\right)\right]. \qquad \text{(A21)}
\end{aligned}$$

A.2 Reduction of synchronous solutions

For a periodic synchronous solution, the phases of all oscillators are equal. Thus, $\eta_{i,j} = 0$ for all i and j. In this instance, (24) becomes

$$\frac{d}{dt}\begin{bmatrix}\phi_1\\ \phi_2\\ \vdots\\ \phi_N\end{bmatrix} = \frac{1}{N}\begin{bmatrix}A+B(0) & B(0) & \dots & B(0)\\ B(0) & A+B(0) & \dots & B(0)\\ \vdots & & \ddots & \vdots\\ B(0) & B(0) & \dots & A+B(0)\end{bmatrix}\begin{bmatrix}\phi_1\\ \phi_2\\ \vdots\\ \phi_N\end{bmatrix}. \tag{A22}$$

Above, the index on A is dropped for notational convenience since the diagonal entries are identical. Much like for periodic splay solutions, the matrix from (24) is circulant so that the eigenvalues and eigenvectors can be found using (A16) and (A17). Recall from (A7) that the row sums are equal to zero so that $\lambda_N = 0$ corresponding to $\boldsymbol{v}_N = \frac{1}{\sqrt{N}}[1 \ \dots \ 1]$. All remaining eigenvalues, $\lambda_k = \frac{A}{N}$ for $k = 1, \dots, N-1$ can be found using (A16) and by noting that $\sum_{j=0}^{N-1} \exp(2\pi kj\sqrt{-1}/N) = 0$ for $1 \le k \le N-1$. The corresponding eigenvectors $\boldsymbol{v}_k$ can be found from (A17).

Using the above information, for small coupling, equation (A10) can be used to determine the phase response curve as

$$\boldsymbol{Z}^T(\Theta)\boldsymbol{P}(t) = u(t)Z_V(\Theta). \tag{A23}$$

Note that above, the relationship $\theta_i^{\text{per}}(\Theta) = \Theta$ is used because all oscillators have identical phases. From (A15), one finds that

$$\boldsymbol{I}_j^T(\Theta)\boldsymbol{P}(t) = u(t)Z_V(\Theta)\sum_{k=1}^{N} w_j^k = 0. \tag{A24}$$

Equation (A24) is simplified in its final step by noting that $\boldsymbol{w}_j$ is orthogonal to a vector of all ones. Therefore, the isostable response curves are well approximated by zero for the synchronized solution. Additionally, using (A15)

$$\begin{aligned}\boldsymbol{C}_j^{k\,T}(\Theta)\boldsymbol{P}(t) &= \sum_{i=1}^{N}\left[w_j^i v_k^i Z_V'(\theta_i^{\text{per}}(\Theta))\right]u(t)\\ &= Z_V'(\Theta)u(t)\sum_{i=1}^{N}\left[w_j^i v_k^i\right]\end{aligned} \tag{A25}$$

In the above equation, $\boldsymbol{w}_j^T\boldsymbol{v}_j = 1$ for $j = k$ and zero otherwise. Therefore

$$\boldsymbol{C}_j^{k\,T}(\Theta)\boldsymbol{P}(t) = \begin{cases}u(t)Z_V'(\Theta), & \text{if } j = k,\\ 0, & \text{otherwise.}\end{cases} \tag{A26}$$

A.3 Reduction of rotating block solutions

For a large population of oscillators, the full splay state may be difficult to stabilize. In this case, rotating block solutions may be easier to stabilize, whereby N/G blocks of G oscillators are spaced equally in phase (see, for example, Fig. 1). Here it will be shown that the reduced equations of the rotating block solutions with 2 blocks are markedly similar to those of the splay solution when only 2 oscillators are considered.

For clarity of notation and of the analysis, a 2-block solution (i.e., two rotating blocks, each with $N/2$ oscillators) will be considered, but note that the general argument to follow can be repeated for any number of blocks with analogous results. In this example, the oscillators can be ordered so that M from (A6) can be written with a block circulant structure

$$M = \frac{1}{N}\begin{bmatrix} \Upsilon & Q_1 \\ Q_1 & \Upsilon \end{bmatrix}, \tag{A27}$$

where $\Upsilon \in \mathbb{R}^{\frac{N}{2}\times\frac{N}{2}}$ and $Q_1 \in \mathbb{R}^{\frac{N}{2}\times\frac{N}{2}}$ is given by

$$\Upsilon = \begin{bmatrix} A+B(0) & B(0) & \dots & B(0) \\ B(0) & A+B(0) & \dots & B(0) \\ \vdots & & \ddots & \vdots \\ B(0) & B(0) & \dots & A+B(0) \end{bmatrix}, \quad Q_1 = \begin{bmatrix} B(\pi) & \dots & B(\pi) \\ \vdots & \ddots & \vdots \\ B(\pi) & \dots & B(\pi) \end{bmatrix}, \tag{A28}$$

and A and B are defined in (A5) and the subscripts on A are dropped for notational convenience because they are all identical. To identify the eigenvalues and eigenvectors of (A27), note that Υ is a circulant matrix with eigenvalues and eigenvectors given by (A16) and (A17), respectively. Let $\boldsymbol{v}_{\Upsilon,k}$ correspond to the kth eigenvector of Υ found according to (A17). One can then verify that because there are $\frac{N}{2}-1$ eigenvectors of Υ in the null space of Q_1, M has $N-2$ eigenvectors of the form

$$\boldsymbol{v}_2 = \begin{bmatrix} \boldsymbol{v}_{\Upsilon,1} \\ \mathbf{0} \end{bmatrix}, \dots, \boldsymbol{v}_{\frac{N}{2}} = \begin{bmatrix} \boldsymbol{v}_{\Upsilon,\frac{N}{2}-1} \\ \mathbf{0} \end{bmatrix}, \boldsymbol{v}_{\frac{N}{2}+1} = \begin{bmatrix} \mathbf{0} \\ \boldsymbol{v}_{\Upsilon,1} \end{bmatrix}, \dots, \boldsymbol{v}_{N-1} = \begin{bmatrix} \mathbf{0} \\ \boldsymbol{v}_{\Upsilon,\frac{N}{2}-1} \end{bmatrix}, \tag{A29}$$

where $\mathbf{0}$ is an appropriately sized vector of zeros. For each of the eigenvectors in (A29), the corresponding eigenvalue is $\lambda_k = \frac{A}{N}$ for $k = 2, \dots, N-1$ (identical to the corresponding eigenvalues of Υ). M has an additional eigenvector

$$\boldsymbol{v}_1 = \frac{1}{\sqrt{N}}\begin{bmatrix} \mathbf{1} \\ -\mathbf{1} \end{bmatrix}, \tag{A30}$$

with corresponding eigenvalue $\lambda_1 = \frac{A}{N} + \frac{1}{2}B(0) - \frac{1}{2}B(\pi)$.

Recalling from (A7) that the row sums of M are equal to zero, the final eigenvector is $\boldsymbol{v}_N = \frac{1}{\sqrt{N}}[\mathbf{1} \mid \mathbf{1}]^T$ with a corresponding eigenvalue of 0. The eigenvectors of M

form an orthonormal set so that $\boldsymbol{w}_k = \boldsymbol{v}_k$ for all k. With this information, one can now use the relationships (A10) and (A15) to approximate the terms of the reduction (5) for the rotating block solutions. From (A10), the phase response curve is well approximated by

$$\begin{aligned}\boldsymbol{Z}^T(\Theta)\boldsymbol{P}(t) &= \frac{u(t)}{N}\sum_{j=1}^{N}\left[Z_V(\theta_j^{\text{per}}(\Theta))\right], \\ &= \frac{u(t)}{2}\left[Z_V(\Theta) + Z_V(\Theta+\pi)\right]. \end{aligned} \tag{A31}$$

In the second line above, the relationship $\theta_j^{\text{per}} = \Theta$ for $i \leq N/2$ and $\theta_j^{\text{per}} = \Theta + \pi$ otherwise has been used. Considering the isostable coordinates associated with $\boldsymbol{v}_1$, using (A15) and simplifying yields a relationship of the form

$$\boldsymbol{I}_k^T(\Theta)\boldsymbol{P}(t) = \begin{cases} \frac{u(t)\sqrt{N}}{2}\left[Z_V(\Theta) - Z_V(\Theta+\pi)\right], & \text{if } k = 1, \\ Z_V(\Theta)\boldsymbol{v}_{\Upsilon,k-1}^T\mathbf{1}, & \text{if } k = 2 \leq k \leq N/2, \\ Z_V(\Theta+\pi)\boldsymbol{v}_{\Upsilon,k-N/2}^T\mathbf{1}, & \text{if } k = N/2+1 \leq k \leq N-1. \end{cases} \tag{A32}$$

Evaluating (A32) by recalling that the eigenvectors $\boldsymbol{v}_{\Upsilon,j}$ are orthogonal to $\mathbf{1}$ for $j = 1, \ldots, \frac{N}{2} - 1$, one finds

$$\boldsymbol{I}_k^T(\Theta)\boldsymbol{P}(t) = \begin{cases} \frac{u(t)\sqrt{N}}{2}\left[Z_V(\Theta) - Z_V(\Theta+\pi)\right], & \text{if } k = 1, \\ 0, & \text{otherwise.} \end{cases} \tag{A33}$$

Note here that the $\boldsymbol{I}_1^T(\Theta)\boldsymbol{P}(t)$ is identical for both the 2-rotating block solution and the 2-oscillator splay state. Additionally from (A15) one finds

$$\boldsymbol{C}_j^{k\,T}(\Theta)\boldsymbol{P}(t) = u(t)Z_V'(\Theta)\sum_{i=1}^{N/2}\left[w_j^i v_k^i\right] + u(t)Z_V'(\Theta+\pi)\sum_{i=N/2+1}^{N}\left[w_j^i v_k^i\right]. \tag{A34}$$

Due to the structure of the eigenvectors in (A29) and (A30), recalling that $\boldsymbol{w}_k$ is equivalent to $\boldsymbol{v}_k$, both sums from (A34) are zero for all $j \neq k$. The remaining sums can be evaluated to find

$$\boldsymbol{C}_j^{k\,T}(\Theta)\boldsymbol{P}(t) = \begin{cases} \frac{u(t)}{2}Z_V'(\Theta) + \frac{u(t)}{2}Z_V'(\Theta+\pi), & \text{if } j = k = 1, \\ u(t)Z_V'(\Theta), & \text{if } j = k \text{ and } 2 \leq j \leq \mathrm{N}/2, \\ u(t)Z_V'(\Theta+\pi), & \text{if } j = k \text{ and } N/2+1 \leq j \leq \mathrm{N}-1, \\ 0, & \text{otherwise.} \end{cases} \tag{A35}$$

A.3.1 Similarity between rotating block and splay state solutions

The 2-rotating block solutions have similar reduced dynamics as the $N = 2$ splay solution. Comparing (A31) and (A20), the 2-rotating block state has a PRC that is identical to that of the 2-oscillator splay state. Additionally, considering λ_1 of the rotating block state:

$$\begin{aligned}\lambda_1 &= \frac{A}{N} + \frac{1}{2}B(0) - \frac{1}{2}B(\pi) \\ &= \frac{1}{2T}\int_0^T \Big[Z_V'(\omega t) f(\omega t, \omega t) + Z_V(\omega t) f_a(\omega t, \omega t) + Z_V'(\omega t) f(\omega t, \omega t + \pi) \\ &\quad + Z_V(\omega t) f_a(\omega t, \omega t + \pi) \Big] dt + \frac{1}{2}B(0) - \frac{1}{2}B(\pi), \end{aligned} \tag{A36}$$

which comparing with (A16) is the same as the principal eigenvalue of the 2-oscillator splay state. The associated functions $\boldsymbol{I}_1^T \boldsymbol{P}(t) = 0$ and $\boldsymbol{C}_1^{1^T} \boldsymbol{P}(t)$ are also identical. The main difference between the $N = 2$ splay solution and the 2-rotating block state is addition of dynamics for neurons within each block. These reduced equations themselves are similar to the behavior of the synchronized solutions, e.g., with the value of $\boldsymbol{I}_k^T \boldsymbol{P}(t) = 0$ for $k \geq 2$ (all modes associated with the individual blocks) and $\boldsymbol{C}_j^{k^T} \boldsymbol{P}(t)$ being proportional to the first derivative of the PRCs of the individual neurons in the second and third lines of (A35).

Appendix B Optimally achieving stabilization and destabilization conditions

Section 4 gives sets of conditions (34), (40), and (43) required to stabilize splay and rotating block solutions and destabilize synchronous solutions, respectively. Here, a method is given to illustrate how to achieve these conditions optimally. This method is adapted from a methodology presented in Wilson (2019b).

To begin, all constraints given in (34), (40), and (43) can be written in the general form

$$x_i + \frac{1}{T_p}\int_0^{T_p} g_i(H_0 + \Omega_p t) u(t) dt = y_i, \text{ for } i = 1, \ldots, n, \tag{B1}$$

where g_i is a general function, y_i, x_i, Ω_p, and H_0 are constants, and n is the number of constraints to be satisfied. Constraints of the form (B1) can be rewritten as differential equations

$$\dot{W}_i = g_i(H_0 + \Omega_p t) u(t), \tag{B2}$$

subject to boundary conditions $W_i(0) = 0$ and $W_i(T_p) = (y_i - x_i)T_p$. In this context, finding an energy-optimal stimulus which satisfies the n conditions from (B1) can be

posed as a calculus of variations problem (Kirk 1998) by finding the stimulus $u(t)$ which minimizes the functional

$$\begin{aligned}&\mathcal{M}[W_1,\ldots,W_n,\dot{W}_1,\ldots,\dot{W}_n,u(t)]\\&\quad=\int_0^{T_p}\left(u^2(t)+\sum_{i=1}^{n}L_i\left[\dot{W}_i-g_i(H_0+\Omega_p t)u(t)\right]\right)dt,\end{aligned}\tag{B3}$$

where L_i are Lagrange multipliers which force the dynamics to satisfy (B2). As in Kirk (1998), Euler–Lagrange equations are

$$\frac{\partial\mathcal{M}}{\partial u}=\frac{d}{dt}\left(\frac{\partial\mathcal{M}}{\partial\dot{u}}\right),\tag{B4}$$

$$\frac{\partial\mathcal{M}}{\partial W_i}=\frac{d}{dt}\left(\frac{\partial\mathcal{M}}{\partial\dot{W}_i}\right),\ i=1,\ldots,n.\tag{B5}$$

Optimal solutions of the functional (B3) will satisfy these Euler–Lagrange equations with boundary conditions given just after (B2). Direct evaluation of (B5) shows that the time derivatives of all Lagrange multipliers are zero which implies $L_i(t)=L_i(0)$ for all i and t. Subsequent evaluation of (B4) shows that the optimal stimulus takes the form

$$u(t)=\sum_{i=1}^{n}\left(\frac{L_i g_i(H_0+\Omega_p t)}{2}\right),\tag{B6}$$

Additionally, from evaluation of the Euler–Lagrange equations, all optimal stimuli will satisfy (B2). As in Wilson (2019b), substituting (B6) into (B2) and manipulating yields n linear equations of the form

$$\begin{bmatrix}y_1-x_1\\\vdots\\y_n-x_n\end{bmatrix}=\frac{1}{2T_p}\begin{bmatrix}\langle g_1,g_1\rangle&\ldots&\langle g_1,g_n\rangle\\\vdots&&\vdots\\\langle f_n,f_1\rangle&\ldots&\langle f_n,f_n\rangle\end{bmatrix}\begin{bmatrix}L_1\\\vdots\\L_n\end{bmatrix},\tag{B7}$$

with $\langle f_i,f_j\rangle\equiv\int_0^{T_p}f_i(\Omega_p t)f_j(\Omega_p t)dt$. Once the Lagrange multiplers have been determined by solving (B7), the optimal stimulus can be computed from (B6).

References

Adamchic I, Hauptmann C, Barnikol UB, Pawelczyk N, Popovych O, Barnikol TT, Silchenko A, Volkmann J, Deuschl G, Meissner WG, Maarouf M, Sturm V, Freund HJ, Tass PA (2014) Coordinated reset neuromodulation for Parkinson's disease: proof-of-concept study. Mov Disord 29(13):1679–1684

Ammari R, Bioulac B, Garcia L, Hammond C (2011) The subthalamic nucleus becomes a generator of bursts in the dopamine-depleted state. Its high frequency stimulation dramatically weakens transmission to the globus pallidus. Front Syst Neurosci 5:43

Anderson RW, Farokhniaee A, Gunalan K, Howell B, McIntyre CC (2018) Action potential initiation, propagation, and cortical invasion in the hyperdirect pathway during subthalamic deep brain stimulation. Brain Stimul 11(5):1140–1150

Ashwin P, Swift JW (1992) The dynamics of n weakly coupled identical oscillators. J Nonlinear Sci 2(1):69–108

Bar-Gad I, Elias S, Vaadia E, Bergman H (2004) Complex locking rather than complete cessation of neuronal activity in the globus pallidus of a 1-methyl-4-phenyl-1, 2, 3, 6-tetrahydropyridine-treated primate in response to pallidal microstimulation. J Neurosci 24(33):7410–7419

Benabid AL, Pollak P, Hoffmann D, Gervason C, Hommel M, Perret JE, De Rougemont J, Gao DM (1991) Long-term suppression of tremor by chronic stimulation of the ventral intermediate thalamic nucleus. Lancet 337(8738):403–406

Benabid AL, Chabardes S, Mitrofanis J, Pollak P (2009) Deep brain stimulation of the subthalamic nucleus for the treatment of Parkinson's disease. Lancet Neurol 8(1):67–81

Brown P, Oliviero A, Mazzone P, Insola A, Tonali P, Di Lazzaro V (2001) Dopamine dependency of oscillations between subthalamic nucleus and pallidum in Parkinson's disease. J Neurosci 21(3):1033–1038

Brown E, Moehlis J, Holmes P (2004) On the phase reduction and response dynamics of neural oscillator populations. Neural Comput 16(4):673–715

Cleary DR, Raslan AM, Rubin JE, Bahgat D, Viswanathan A, Heinricher MM, Burchiel KJ (2013) Deep brain stimulation entrains local neuronal firing in human globus pallidus internus. J Neurophysiol 109(4):978–987

Ermentrout GB, Terman DH (2010) Mathematical foundations of neuroscience, vol 35. Springer, New York

Eusebio A, Thevathasan W, Gaynor LD, Pogosyan A, Bye E, Foltynie T, Zrinzo L, Ashkan K, Aziz T, Brown P (2011) Deep brain stimulation can suppress pathological synchronisation in parkinsonian patients. J Neurol Neurosurg Psychiatry 82(5):569–573

Gardiner CW (2004) Handbook of stochastic methods: for physics, chemistry and the natural sciences. Springer, Berlin

Grimshaw R (1993) Nonlinear ordinary differential equations, vol 2. CRC Press, Baca Raton

Guckenheimer J (1975) Isochrons and phaseless sets. J Math Biol 1(3):259–273

Guckenheimer J, Holmes P (1983) Nonlinear oscillations, dynamical systems, and bifurcations of vector fields, vol 42. Springer, New York

Hahn PJ, Russo GS, Hashimoto T, Miocinovic S, Xu W, McIntyre CC, Vitek JL (2008) Pallidal burst activity during therapeutic deep brain stimulation. Exp Neurol 211(1):243–251

Hammond C, Bergman H, Brown P (2007) Pathological synchronization in Parkinson's disease: networks, models and treatments. Trends Neurosci 30:357–64

Hashimoto E, Elder CM, Okun MS, Patrick SK, Vitek JL (2003) Stimulation of the subthalamic nucleus changes the firing pattern of pallidal neurons. J Neurosci 23(5):1916–1923

Hespanha JP (2018) Linear systems theory. Princeton University Press, Princeton

Holt AB, Netoff TI (2014) Origins and suppression of oscillations in a computational model of Parkinson's disease. J Comput Neurosci 37(3):505–521

Izhikevich EM (2007) Dynamical systems in neuroscience: the geometry of excitability and bursting. MIT Press, London

Johnston D, Wu SM-S (1995) Foundations of cellular neurophysiology. MIT Press, Cambridge

Jordan D, Smith P (2007) Nonlinear ordinary differential equations: an introduction for scientists and engineers, vol 10. Oxford University Press, Oxford

Kane A, Hutchison WD, Hodaie M, Lozano AM, Dostrovsky JO (2009) Enhanced synchronization of thalamic theta band local field potentials in patients with essential tremor. Exp Neurol 217(1):171–176

Kawamura Y, Nakao H, Arai K, Kori H, Kuramoto Y (2008) Collective phase sensitivity. Phys Rev Lett 101(2):024101

Kirk D (1998) Optimal control theory. Dover Publications, New York

Ko TW, Ermentrout GB (2009) Phase-response curves of coupled oscillators. Phys Rev E 79(1):016211

Kotani K, Yamaguchi I, Yoshida L, Jimbo Y, Ermentrout GB (2014) Population dynamics of the modified theta model: macroscopic phase reduction and bifurcation analysis link microscopic neuronal interactions to macroscopic gamma oscillation. J R Soc Interface 11(95):20140058

Kra I, Simanca SR (2012) On circulant matrices. Not AMS 59(3):368–377

Kühn AA, Kempf F, Brücke C, Doyle LG, Martinez-Torres I, Pogosyan A, Trottenberg T, Kupsch A, Schneider GH, Hariz MI, Vandenberghe W, Nuttin B, Brown P (2008) High-frequency stimulation of the subthalamic nucleus suppresses oscillatory β activity in patients with Parkinson's disease in parallel with improvement in motor performance. J Neurosci 28(24):6165–6173

Kühn AA, Tsui A, Aziz T, Ray N, Brücke C, Kupsch A, Schneider GH, Brown P (2009) Pathological synchronisation in the subthalamic nucleus of patients with Parkinson's disease relates to both bradykinesia and rigidity. Exp Neurol 215(2):380–387

Kuncel AM, Grill WM (2004) Selection of stimulus parameters for deep brain stimulation. Clin Neurophysiol 115(11):2431–2441

Kuramoto Y (1984) Chemical oscillations, waves, and turbulence. Springer, Berlin

Levnajić Z, Pikovsky A (2010) Phase resetting of collective rhythm in ensembles of oscillators. Phys Rev E 82(5):056202

Levy R, Hutchison WD, Lozano AM, Dostrovsky JO (2002) Synchronized neuronal discharge in the basal ganglia of parkinsonian patients is limited to oscillatory activity. J Neurosci 22(7):2855–2861

Little S, Pogosyan A, Neal S, Zavala B, Zrinzo L, Hariz M, Foltynie T, Limousin P, Ashkan K, FitzGerald J, Green AL, Aziz TZ, Brown P (2013) Adaptive deep brain stimulation in advanced Parkinson disease. Ann Neurol 74(3):449–457

Manos T, Zeitler M, Tass PA (2018) How stimulation frequency and intensity impact on the long-lasting effects of coordinated reset stimulation. PLoS Comput Biol 14(5):e1006113

Matchen TD, Moehlis J (2018) Phase model-based neuron stabilization into arbitrary clusters. J Comput Neurosci 44(3):363–378

McIntyre CC, Mori S, Sherman DL, Thakor NV, Vitek JL (2004) Electric field and stimulating influence generated by deep brain stimulation of the subthalamic nucleus. Clin Neurophysiol 115(3):589–595

Monga B, Moehlis J (2019) Phase distribution control of a population of oscillators. Physica D Nonlinear Phenom 398:115–129

Monga B, Wilson D, Matchen T, Moehlis J (2019) Phase reduction and phase-based optimal control for biological systems: a tutorial. Biol Cybern 113(1–2):11–46

Moro E, Esselink RJA, Xie J, Hommel M, Benabid AL, Pollak P (2002) The impact on Parkinson's disease of electrical parameter settings in STN stimulation. Neurology 59(5):706–713

Nabi A, Mirzadeh M, Gibou F, Moehlis J (2013) Minimum energy desynchronizing control for coupled neurons. J Comput Neurosci 34:259–271

Nakao H, Arai K, Kawamura Y (2007) Noise-induced synchronization and clustering in ensembles of uncoupled limit-cycle oscillators. Phys Rev Lett 98(18):184101

Nakao H, Yasui S, Ota M, Arai K, Kawamura Y (2018) Phase reduction and synchronization of a network of coupled dynamical elements exhibiting collective oscillations. Chaos Interdiscip J Nonlinear Sci 28(4):045103

Perlmutter JS, Mink JW (2006) Deep brain stimulation. Annu Rev Neurosci 29:229–257

Priori A, Foffani G, Pesenti A, Tamma F, Bianchi AM, Pellegrini M, Locatelli M, Moxon KA, Villani RM (2004) Rhythm-specific pharmacological modulation of subthalamic activity in Parkinson's disease. Exp Neurol 189(2):369–379

Rosa M, Giannicola G, Servello D, Marceglia S, Pacchetti C, Porta M, Sassi M, Scelzo E, Barbieri S, Priori A (2011) Subthalamic local field beta oscillations during ongoing deep brain stimulation in Parkinson's disease in hyperacute and chronic phases. Neurosignals 19(3):151–162

Rosa M, Arlotti M, Ardolino G, Cogiamanian F, Marceglia S, Di Fonzo A, Cortese F, Rampini PM, Priori A (2015) Adaptive deep brain stimulation in a freely moving parkinsonian patient. Mov Disord 30(7):1003–1005

Rubin J, Terman D (2004) High frequency stimulation of the subthalamic nucleus eliminates pathological thalamic rhythmicity in a computational model. J Comput Neurosci 16:211–235

Sanders JA, Verhulst F, Murdock J (2007) Averaging methods in nonlinear dynamical systems, 2nd edn. Springer, New York

Tass PA (2003) A model of desynchronizing deep brain stimulation with a demand-controlled coordinated reset of neural subpopulations. Biol Cybern 89(2):81–88

Tass PA, Qin L, Hauptmann C, Dovero S, Bezard E, Boraud T, Meissner WG (2012) Coordinated reset has sustained aftereffects in parkinsonian monkeys. Ann Neurol 72(5):816–820

Tsang EW, Hamani C, Moro E, Mazzella F, Saha U, Lozano AM, Hodaie M, Chuang R, Steeves T, Lim SY, Neagu B, Chen R (2012) Subthalamic deep brain stimulation at individualized frequencies for Parkinson disease. Neurology 78(24):1930–1938

Volkmann J, Herzog J, Kopper F, Deuschl G (2002) Introduction to the programming of deep brain stimulators. Mov Disord 17(S3):S181–S187

Wang J, Nebeck S, Muralidharan A, Johnson MD, Vitek JL, Baker KB (2016) Coordinated reset deep brain stimulation of subthalamic nucleus produces long-lasting, dose-dependent motor improvements in the 1-methyl-4-phenyl-1, 2, 3, 6-tetrahydropyridine non-human primate model of parkinsonism. Brain Stimul 9(4):609–617

Wilson D (2019a) Isostable reduction of oscillators with piecewise smooth dynamics and complex Floquet multipliers. Phys Rev E 99(2):022210

Wilson D (2019b) An optimal framework for nonfeedback stability control of chaos. SIAM J Appl Dyn Syst 18(4):1982–1999

Wilson D, Ermentrout B (2018) Greater accuracy and broadened applicability of phase reduction using isostable coordinates. J Math Biol 76(1–2):37–66

Wilson D, Ermentrout B (2019) Augmented phase reduction of (not so) weakly perturbed coupled oscillators. SIAM Rev 61(2):277–315

Wilson D, Moehlis J (2014) Optimal chaotic desynchronization for neural populations. SIAM J Appl Dyn Syst 13(1):276–305

Wilson D, Moehlis J (2015) Clustered desynchronization from high-frequency deep brain stimulation. PLoS Comput Biol 11(12):e1004673

Wilson C, Beverlin II B, Netoff T (2011) Chaotic desynchronization as the therapeutic mechanism of deep brain stimulation. Front Syst Neurosci 5:Art. No. 50

Winfree A (2001) The geometry of biological time, 2nd edn. Springer, New York